Available online at www.sciencedirect.com
ScienceDirect
Bioorganic & Medicinal Chemistry
ELSEVIER
Bioorganic & Medicinal Chemistry 15 (2007) 6810–6818

Identification of novel chemical inhibitors for ubiquitin C-terminal hydrolase-L3 by virtual screening

Kazunori Hirayama,[a,b] Shunsuke Aoki,[b,*] Kaori Nishikawa,[b] Takashi Matsumoto[a] and Keiji Wada[b]

[a]*Department of Electrical Engineering and Bioscience, Graduate School of Advanced Science and Engineering, Waseda University, 3-4-1 Okubo, Shinjuku-ku, Tokyo 169-8555, Japan*
[b]*Department of Degenerative Neurological Diseases, National Institute of Neuroscience, National Center of Neurology and Psychiatry, 4-1-1 Ogawa-Higashi, Kodaira, Tokyo 187-8502, Japan*

Received 11 May 2007; revised 14 July 2007; accepted 18 July 2007
Available online 19 August 2007

Abstract—UCH-L3 (ubiquitin C-terminal hydrolase-L3) is a de-ubiquitinating enzyme that is a component of the ubiquitin–proteasome system and known to be involved in programmed cell death. A previous study of high-throughput drug screening identified an isatin derivative as a UCH-L3 inhibitor. In this study, we attempted to identify a novel inhibitor with a different structural basis. We performed in silico structure-based drug design (SBDD) using human UCH-L3 crystal structure data (PDB code; 1XD3) and the virtual compound library (ChemBridge CNS-Set), which includes 32,799 chemicals. By a two-step virtual screening method using DOCK software (first screening) and GOLD software (second screening), we identified 10 compounds with GOLD scores of over 60. To address whether these compounds exhibit an inhibitory effect on the de-ubiquitinating activity of UCH-L3, we performed an enzymatic assay using ubiquitin-7-amido-4-methylcoumarin (Ub-AMC) as the substrate. As a result, we identified three compounds with similar basic dihydro-pyrrole skeletons as UCH-L3 inhibitors. These novel compounds may be useful for the research of UCH-L3 function, and in drug development for UCH-L3-associated diseases.

1. Introduction

The ubiquitin–proteasome system is responsible for the regulation of cellular proteolysis. In this system, ubiquitination serves as a targeting signal for proteolysis.[1] Ubiquitin C-terminal hydrolase-L3 (UCH-L3) is one of the components of the ubiquitin–proteasome system and hydrolyzes ubiquitin C-terminal adducts for the recycling of cellular ubiquitin.[2] Ubiquitin with C-terminal adducts is a substrate for UCH-L3, and ubiquitin with a free C-terminus is recycled within the ubiquitin–proteasome system. There is some evidence that UCH-L3 plays an important role in programmed cell death. Programmed cell death is implicated in a number of human diseases, including neurodegenerative disease,[3] autoimmune disease,[4] cancers[5,6], etc. Loss of UCH-L3 leads to programmed cell death by apoptosis of certain type of cells in vivo, germ line cells and photoreceptor cells.[7,8] High-level expression of UCH-L3 genes and proteins, and acceleration of UCH-L3 enzymatic activity is reported in multiple types of cancer cells,[5,6] suggesting that UCH-L3 activity may be required for cancer cell survival. Therefore, UCH-L3 is a potential target for drug development to control programmed cell death in specific types of cells including cancer cells.

Structure-based drug design (SBDD) is a method used to discover novel leads for drug development as it enables more rapid hit identification than the classical screening methods of in vitro or in vivo biological assays. The computer-based approach for drug screening, using molecular docking, is a shortcut method when the crystal structure of a target protein is available. Key methodologies for docking small molecules to protein were developed during the early 1980s,[9] and various types of docking simulation software are now available, for example, DOCK,[10] GOLD, and FlexX.[11] BCR-ABL tyrosine kinase inhibitors (IC_{50} values ranging from 10 to 200 μM) were successfully

Keywords: UCH-L3; Dihydro-pyrrole; Structure-based drug design; Virtual screening.
* Corresponding author. Tel.: +81 42 341 2712x5144; fax: +81 42 346 1745; e-mail: aokis@ncnp.go.jp

0968-0896/$ - see front matter © 2007 Elsevier Ltd. All rights reserved.
doi:10.1016/j.bmc.2007.07.016

identified by virtual screening of 200,000 compounds against crystal structures using DOCK,[12] implemented by the anchor-and-grow algorithm with respect to ligand flexibility.[10] Human thymidine phosphorylase inhibitor (IC_{50} = 77 μM) was also identified by virtual screening of 250,521 compounds using DOCK.[13] Furthermore, metallo-β-lactamase inhibitors (IC_{50} values less than 15 μM) were identified through virtual screening by GOLD,[14] using the genetic algorithm for ligand flexibility.

The advantage of chaining different docking programs was evaluated and the results suggested that virtual ligand screening is performed faster with reasonable accuracy by using chained screening, than by using a single program with default parameters.[15] In this study, the results of chained docking against UCH-L3 crystal structure were examined by UCH-L3 hydrolysis activity assay to validate the efficacy of the DOCK–GOLD SBDD method. We identified three inhibitors (IC_{50} = 100–150 μM) of UCH-L3 by the DOCK–GOLD virtual screening of 32,799 compounds.

2. Results and discussion

2.1. Protein preparation and chemical database

In the 3D structure of the UCH-L3-ubiquitin complex, ubiquitin C-terminus is buried in the active site cleft among four active site residues of UCH-L3: Gln89, Cys95, His169, and Asp184.[16,17] During the virtual screening process by DOCK and GOLD, the protein–ligand interacting site was restricted to the binding site of the three ubiquitin C-terminal amino residues (as described in Section 4), in order that the outcome could be verified by a ubiquitin C-terminal hydrolase enzymatic assay. The first DOCK screening was performed against 32,799 compounds of CNS-Set, which was prefiltered by RPBS under the most modest filtering condition.[18]

2.2. DOCK and GOLD screenings

To screen for compounds that bind to the active site, the first screening was performed by DOCK, and the protein–ligand interaction area was restricted to the ubiquitin binding site of UCH-L3 (see Section 4). The top-scoring 1780 compounds (5.4% of the initial 32,799 compounds) with energy scores of less than −30 kcal/mol were selected for further screening. These compounds were then re-screened by GOLD twice, with different genetic algorithm (GA) settings. To predict binding ability to the active site cleft accurately, the protein–ligand interacting area was defined in approximately the same way as in the first DOCK screening step (see Section 4). Screening by GOLD consisted of two rounds. Using the GOLD score, we initially extracted the top scoring 100 compounds from 1780 compounds, using the 7–8 times speed-up GA parameter settings. These 100 compounds were then re-scored using the default GA settings (see Section 4) to more accurately predict binding ability. Ten compounds with GOLD scores of over 60 were predicted to bind to the UCH-L3 active site; that is, 0.03% of the total number of chemical compounds was screened.

2.3. IC_{50} determination

A previous study demonstrated that compounds with GOLD scores of about 60 may inhibit enzyme activity with IC_{50} values of 10–100 μM.[19] An enzyme assay was performed among the top 10 chemicals to address whether they actually bind to the UCH-L3 active site with the predicted affinities (Table 1 and Fig. 1).

Ubiquitin-7-amido-4-methylcoumarin (Ub-AMC; AMC attaches to the carboxyl terminus of ubiquitin) is a fluorogenic substrate of UCH-L3 and other UCH isozymes. UCH-L3 is known to hydrolyze Ub-AMC into free ubiquitin and AMC,[20,21] and the hydrolyzed AMC group is excited at light wavelength of 355 nm and emits fluorescence at 460 nm. Hydrolysis activity of UCH-L3 is inhibited if a compound binds to its active site and thus blocks interaction between the active site of UCH-L3 and the ubiquitin C-terminus. Inhibition of hydrolysis of Ub-AMC leads to a lower concentration of free AMC and hence a lower level of fluorescence intensity.

We experimentally determined the affinity constant (K_m) of Ub-AMC hydrolysis by human UCH-L3 as 83.3 ± 1.5 nM (mean ± SEM, from three independent experiments). The candidate compounds identified by

Table 1. GOLD scores of the top 10 ranked chemicals after GOLD calculation[a]

Docking rank/Compound No.	Compound name	GOLD scores
1	1-Benzyl-3-hydroxy-4-(5-methyl-2-furoyl)-5-(3-pyridinyl)-1,5-dihydro-2*H*-pyrrol-2-one	66.01
2	3-[4-Methyl-5-({[3-(2-thienyl)-1,2,4-oxadiazol-5-yl]methyl}thio)-4*H*-1,2,4-triazol-3-yl]-1*H*-indole	65.62
3	*N*-{4-[1-(2-Furoyl)-5-(2-furyl)-4,5-dihydro-1*H*-pyrazol-3-yl]phenyl}methanesulfonamide	64.85
4	N^1-Cyclopropyl-N^2-(4-methoxyphenyl)-N^2-[(4-methylphenyl)sulfonyl]glycinamide	64.76
5	*N*-{3-[1-Acetyl-5-(2-thienyl)-4,5-dihydro-1*H*-pyrazol-3-yl]phenyl}ethanesulfonamide	64.23
6	3-Hydroxy-5-(4-methoxyphenyl)-1-(1,3,4-thiadiazol-2-yl)-4-(2-thienylcarbonyl)-1,5-dihydro-2*H*-pyrrol-2-one	62.96
7	5-(4-Fluorophenyl)-3-hydroxy-4-(5-methyl-2-furoyl)-1-(3-pyridinylmethyl)-1,5-dihydro-2*H*-pyrrol-2-one	62.73
8	N^1-Cyclopropyl-N^2-[(4-methoxyphenyl)sulfonyl]-N^2-(4-methylphenyl)glycinamide	62.52
9	N^1-Cyclopentyl-N^2-(3-methoxyphenyl)-N^2-(phenylsulfonyl)glycinamide	62.39
10	4-({[5-(2-Furyl)-4-phenyl-4*H*-1,2,4-triazol-3-yl]thio}methyl)-1,3-thiazol-2-amine	62.35

[a] Ten compounds are listed according to the top 10 rank of GOLD scores and assigned the number corresponding to GOLD score ranks.

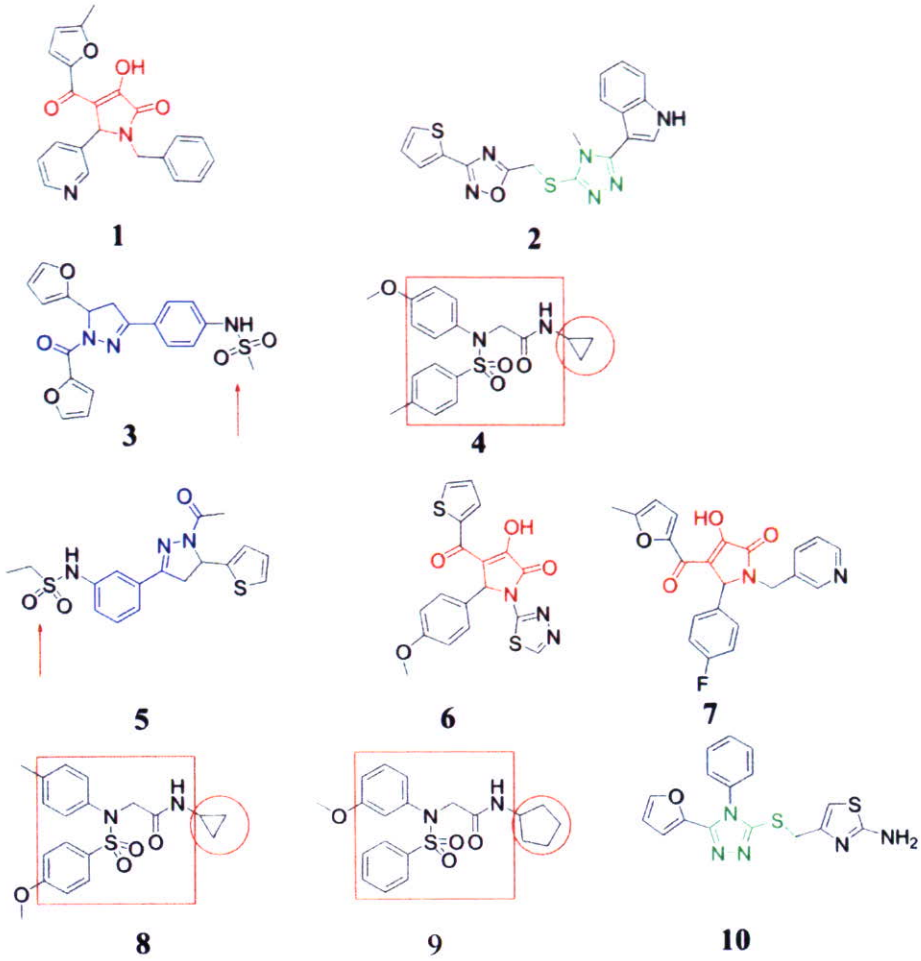

Figure 1. Top 10 ranked compounds identified by DOCK and GOLD screening. Note that there are several shared basic skeletons and functional groups: 1,5-dihydro-2*H*-pyrrol-2-one (drawn in red, compounds **1**, **6**, and **7**), glycinamide (boxed in red, compounds **4**, **8**, and **9**), cycloalkane group (circled in red, compounds **4** and **8**; cyclopropyl, compound **9**; cyclopentyl), 4,5-dihydro-1*H*-pyrazol-3-yl phenyl (drawn in blue, compounds **3** and **5**), sulfonamide (pointed, compounds **3** and **5**), and 4*H*-1,2,4-triazol-3-yl (drawn in green, compounds **2** and **10**).

DOCK–GOLD chained docking screening were tested for their ability to inhibit the hydrolysis activity of UCH-L3, at the Ub-AMC concentration equivalent to the K_m value. Four compounds among these candidates inhibited enzyme activity (Fig. 2a). We did not test the inhibitory effects of compound **3**, as it is a fluorogenic chemical with an emission wavelength of 460 nm. Compounds **1**, **6**, and **7** significantly inhibited the hydrolysis activity of UCH-L3 (initial velocity of Ub-AMC hydrolysis; nM/s [Fig. 2b]). Compounds **1** (401 μM), **6** (375 μM), and **7** (350 μM) inhibited the hydrolysis activity by 83.2 ± 1.5%, 76.5 ± 0.6%, and 76.8 ± 1.0%, respectively, as compared with control DMSO ($p < 0.01$, vs control; Dunnett's test). The IC_{50} value of compound **2** should hypothetically be several hundred μM. Although compound **2** (380 μM) inhibited hydrolysis activity by 16.2 ± 2.1% as compared with control DMSO, the difference was not found to be significant by Dunnett's test. Five other compounds were unable to inhibit the UCH-L3 hydrolysis activity: compound **4** (334 μM; final concentration), compound **5** (331 μM), compound **8** (401 μM), compound **9** (386 μM), and compound **10** (387 μM) (Fig. 2b). Experimentally determined IC_{50} values of compounds **1**, **6**, and **7** (Fig. 3) were as follows: compound **1** (103 μM), compound **6** (154 μM), and compound **7** (123 μM).

2.4. Competitive inhibitor

To show that the identified compounds bind to the active site of the UCH-L3, various concentrations of compound **1** and iodoacetamide (108 mM) were added to UCH-L3/Ub-AMC reaction buffer. Iodoacetamide is a non-competitive inhibitor of UCH-L3 (Fig. 4a). It is a thiol alkylating agent of the UCH-L family and derivatizes and inactivates the active site leading to loss of UCH-L3 enzymatic activity.[22] In the presence of compound **1** and iodoacetamide, the percentage of active UCH-L3 reduced by iodoacetamide treatment was recovered in comparison with the control, and the recovery was dependent on the concentration of compound **1** (Fig. 4b). Our results showed that compound **1** is a competitive inhibitor of UCH-L3. This suggests that compound **1** bound to the UCH-L3 active site to prevent iodoacetamide from inactivating it.

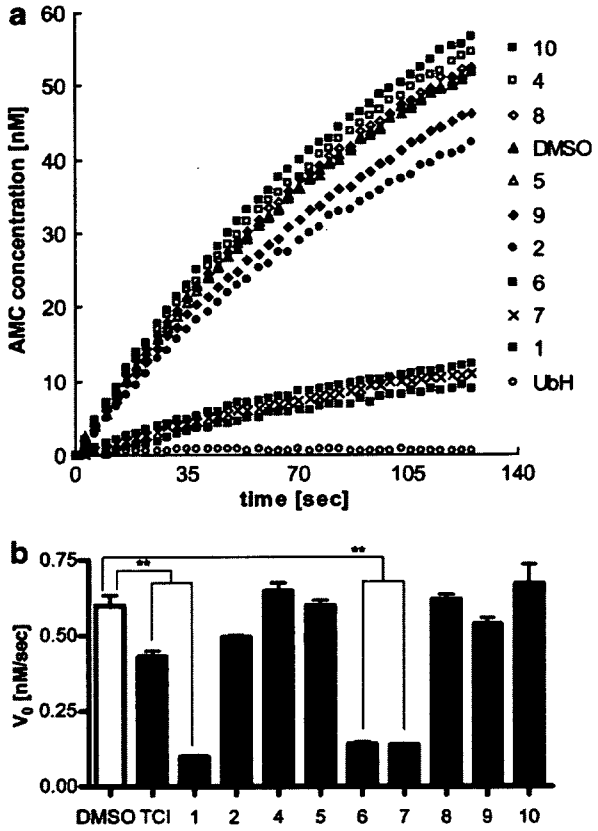

Figure 2. Analysis of UCH-L3 inhibitory effects of compounds 1–10. (a) Kinetics of UCH-L3-catalyzed hydrolysis of Ub-AMC with the compounds. Fluorescence intensity was converted to AMC concentration by subtracting the intensity of fully hydrolyzed substrate from that of solution without substrate. Concentrations of compounds are as follows: compound **1** (401 μM); compound **2** (380 μM); compound **4** (334 μM); compound **5** (331 μM); compound **6** (375 μM); compound **7** (350 μM); compound **8** (401 μM); compound **9** (386 μM); and compound **10** (387 μM). As a known inhibitor, ubiquitin-aldehyde (Ub-H, 120 nM) was used. Each value represents the mean of three independent experiments. (b) Inhibitory effects of compounds on initial velocity of hydrolysis (V_0) are shown. Fluorescence intensity was converted by the same method described in (a). 4,5,6,7-Tetrachloroindan-1,3-dione (TCI, 20 μM) was used as a UCH-L3 selective inhibitor with IC_{50} of 600 nM.[22] Each value represents the mean ± SEM of three independent experiments. Dunnett's multiple comparison test was performed using GraphPad Prism software (**: $p < 0.01$, DMSO as control).[29]

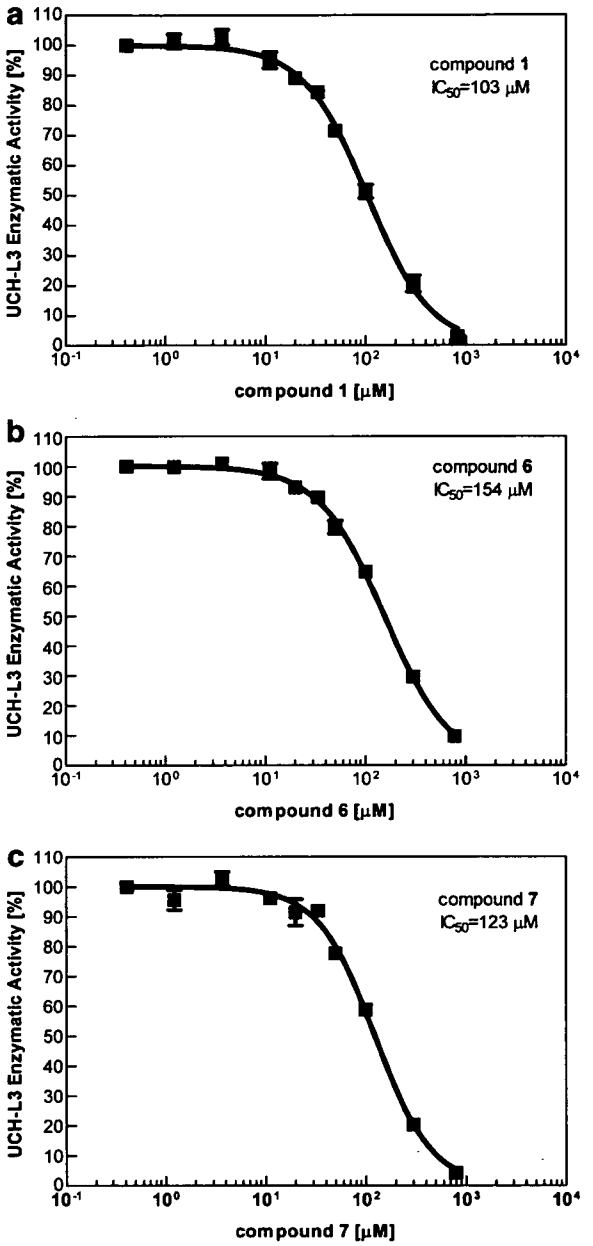

Figure 3. IC_{50} curves of compounds for UCH-L3 enzymatic activity. (a) Compound **1**, (b) compound **6**, and (c) compound **7**. The horizontal axis shows the concentration of each compound. The vertical axis shows the relative UCH-L3 enzymatic activity [%] in comparison with maximal initial velocity. IC_{50} values are shown in graphs. Each plotted value represents the mean ± SEM of three independent experiments.

In order to show that the compounds **1**, **6**, and **7** bind to UCH-L3, Biacore 100 analysis was conducted. Biacore 100 analysis detects interaction between a small molecule and protein and enables quantification of the interaction.[23] The results showed that binding of each compound to UCH-L3 increased and was dependent on the concentration of the compound **6** (data not shown).

2.5. Predicted binding mode

Figure 5 shows the predicted binding modes of compounds **1**, **6**, and **7** to UCH-L3. Since chemical formulae of the three compounds are similar to each other, the predicted docked structures of these and UCH-L3 have similar binding modes. Two hydrogen bonds were observed between the docked ligand and two amino acid residues in the predicted compound **1**/UCH-L3 complex structure; the carbonyl group of compound **1** appears to form a hydrogen bond to the NH group of Ala11, and the pyrrole C=O appears to form a hydrogen bond to the hydroxyl group of Thr157. Three hydrogen bonds were predicted between the docked ligand and two amino acid residues in the compound **6**/UCH-L3 complex structure; the thiadiazole group of compound **6** appears to form a hydrogen bond to the NH group of Leu9, and

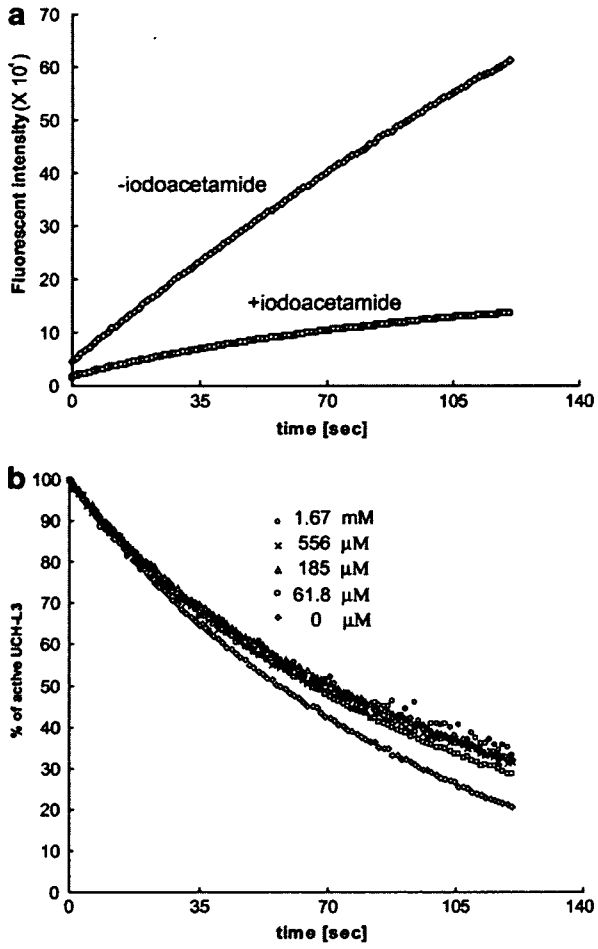

Figure 4. Competitive inhibition of compound 1. (a) Kinetics of UCH-L3-catalyzed hydrolysis of Ub-AMC with or without iodoacetamide (108 mM). (b) Reaction progress curves normalized by final fluorescence intensity representing the ratio of active UCH-L3 (for calculations, see Section 4.9), in the presence of iodoacetamide (108 mM) and compound 1 (0 μM, 61.8 μM, 185 μM, 556 μM, and 1.67 mM).

the pyrrole hydroxyl group and pyrrole C=O appear to form a hydrogen bond to the NH group of Ala11. A hydrogen bond was observed between the docked ligand and the amino acid residues of UCH-L3 in the predicted compound **7**/UCH-L3 complex structure; the carbonyl group of compound **7** appears to form a hydrogen bond to the NH group of Ala11. The predicted binding mode of compound **10**, as a non-binder, was analyzed. Four hydrogen bonds were observed between the docked ligand and the amino acid residues of UCH-L3 in the predicted compound **10**/UCH-L3 complex structure. The triazol group of compound **10** appears to form two hydrogen bonds to the hydroxyl group of Thr157, and the amino group of compound **10** appears to form a hydrogen bond to the CO group of Glu154, and to the CO group of Ser151. Although hydrogen bonds between actual inhibitors (compounds **1**, **6**, and **7**) and Ala11 were observed, compound **10**, a non-inhibitor, does not appear to form a hydrogen bond to Ala11. This hydrogen bond might be important for compounds to bind stably to the UCH-L3 active site.

2.6. Discussion; analysis of active compounds

By three-step virtual screening (DOCK, high-speed GOLD, and low-speed GOLD) of 32,799 chemicals, we identified 10 candidate chemicals that potentially inhibit UCH-L3 hydrolysis activity. We examined the actual inhibitory effects of the compounds on UCH-L3 hydrolysis activity by biochemical enzymatic assay and identified three compounds (compounds **1**, **6**, and **7**) as UCH-L3 inhibitors, with IC_{50} values of 100–150 μM. By comparing the structural formulae of the three compounds, we found that the 1,5-dihydro-2*H*-pyrrol-2-one group is likely to be important for inhibition of UCH-L3-hydrolysis activity (Fig. 6). Several common structural features can be drawn from these three chemicals (Fig. 6). First, the heteroaromatic pyrrole group is common to all three compounds. Second, each of the three compounds also contains pyridines and furoyls as heteroaromatic functional groups. Third, a carbon–oxygen double bond at position 2, a hydroxyl group at position 3, a carbonyl group at position 4, and a hydrogen atom at position 5 of the pyrrole ring are common to each compound. Fourth, a five- or six-membered cyclic group at positions 1, 4, and 5 is common to all three chemicals (Fig. 6). Furthermore, compounds **1** and **7** have two heteroaromatic groups: a pyridinyl group and a furoyl group.

The structural similarities of UCH-L3-binding chemicals have an influence on binding mode similarities. There are two main pockets in the substrate-binding site of UCH-L3: the first pocket (Pocket 1) is formed by Pro8, Glu10, and Thr157 and the second pocket (Pocket 2), the active site pocket, is formed by Asp167, Leu168, and Cys90. Docked orientations of compounds **1** and **7** are very similar, as positions 1 and 5 six-membered cyclic groups fit into each pocket. This suggests that two features among these similarities are likely to be important for stable binding to the active site: a pyrrole ring and two heteroaromatic groups, which fit into both pockets around the UCH-L3 substrate-binding site. The shape of Pocket 1 is different from that of UCH-L1,[24] another isoform of the UCH family (52% amino acid sequence identity).[25] Thus, modification of the chemical groups in Pocket 1 might be effective during drug design, to enhance specificity for UCH-L3 over UCH-L1.

Several lines of evidence indicate that UCH-L3 is associated with tumorigenesis and carcinogenesis. High-level expression and activity of UCH-L3 has been reported in multiple types of cancer cells. Expression of UCH-L3 mRNA is upregulated in breast tumors and UCH-L3 mRNA levels are associated with the histological grading of such tumors.[5] Moreover, it has been suggested that the activity of UCH-L3 is also upregulated in the majority of cervical carcinoma tissues, compared with adjacent normal tissues.[6] On the other hand, loss of UCH-L3 is known to induce cell death in knock-out studies. UCH-L3 is involved in the protection of programmed cell death in germ cells and photoreceptor cells in vivo.[7,8] Thus, the structural information of the

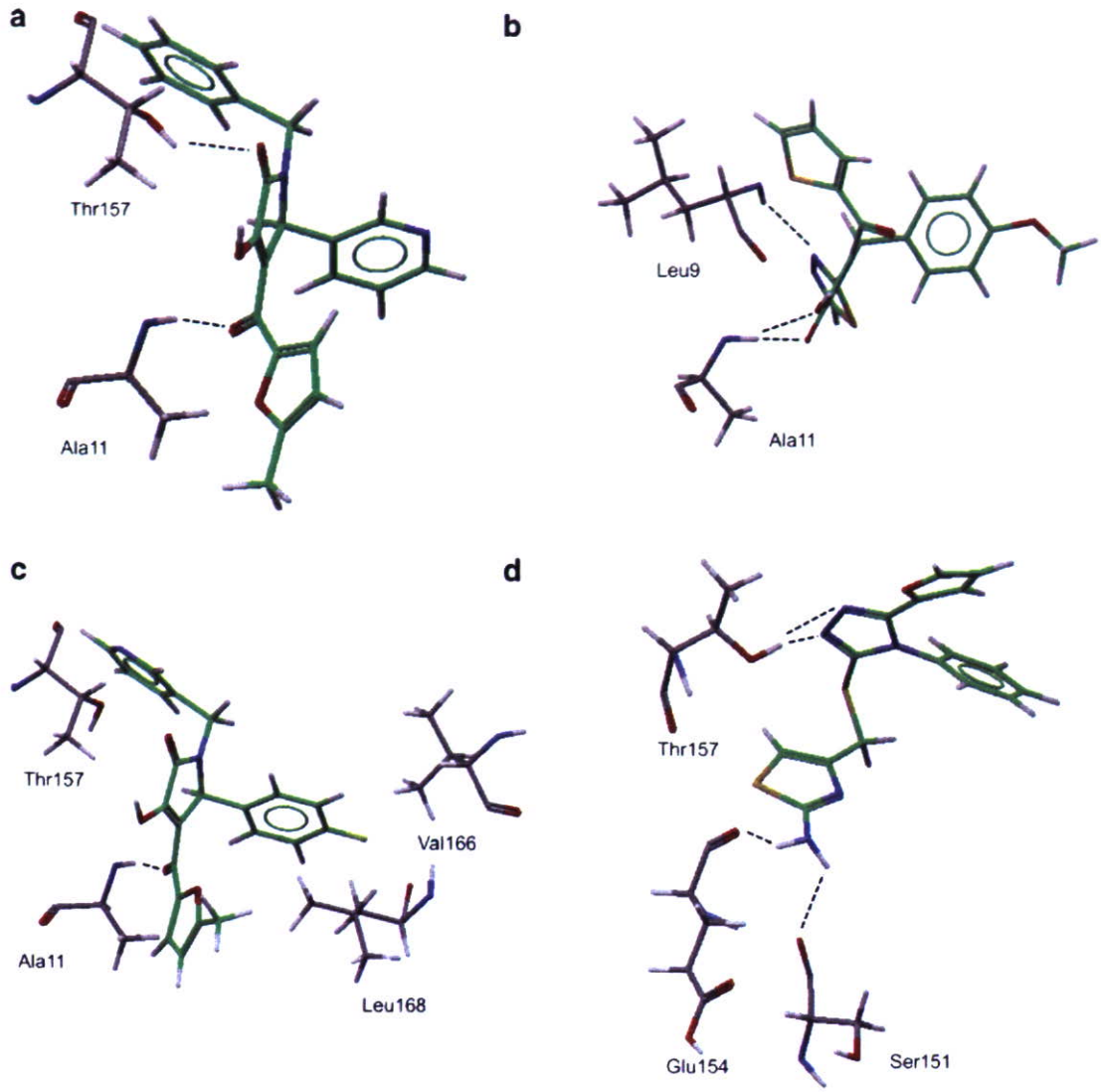

Figure 5. Illustration showing the molecular docking results. Docked orientation of (a) compound **1**, (b) compound **6**, (c) compound **7**, and (d) compound **10** in the UCH-L3 active site using GOLD and shown with interacting residues. Hydrogen bonds are shown by a dashed line. Oxygen atoms are shown in red, nitrogen atoms in blue, sulfur atoms in orange, fluorine atoms in yellow, and hydrogen atoms in gray. The enzyme carbons are shown in dark gray and those of the ligands in green.

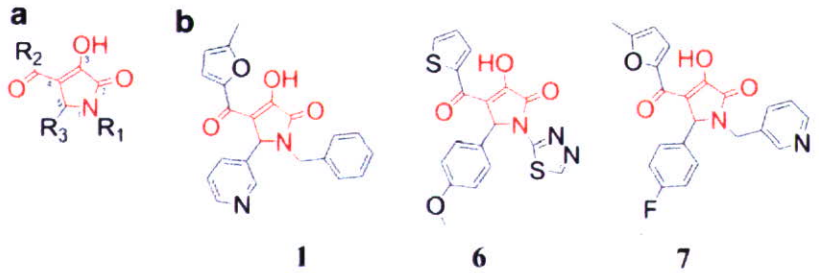

Figure 6. Structural similarities of the three compounds. (a) 1,5-Dihydro-2*H*-pyrrol-2-one group, the common basic skeleton, is shown in red. Position numbers of the pyrrole ring are shown as small characters. R_1–R_3 represent each functional group at positions 1, 4, and 5 of the pyrrole ring, respectively. (b) Structures of identified inhibitors: compounds **1**, **6**, and **7**.

UCH-L3 inhibitors we identified may be useful for future apoptosis-inducing anti-cancer drug development. UCH-L3 should be an important target for modulating cell apoptosis.

3. Conclusion

In this study, we employed three-step docking (DOCK, rough GOLD, and fine GOLD) and in vitro enzyme

assay methods, and identified three UCH-L3 inhibitors with IC_{50} values of 100–150 μM. These novel inhibitors have a dihydro-pyrrole group in common.

4. Experimental

4.1. Compound library

We used the ADME/Tox (absorption, distribution, metabolism, excretion, and toxicity) filtered virtual compound library (ChemBridge CNS-Set) which includes a collection of 32,799 chemical compounds.[18] All compounds satisfy Lipinski's Rule of five.

4.2. Protein preparation

Human UCH-L3 and ubiquitin vinylmethylester (Ub-VME) complex crystal structure data (PDB code; 1XD3) were obtained from Protein Data Bank (PDB).[17] Hydrogens were added to UCH-L3-ubiquitin complex using CVFF99 force field by Biopolymer module in Insight II 2000 suite (Accelrys, Inc., San Diego, CA). Energy was minimized by the Discover 3 module of the same suite with all heavy atoms restrained, except hydrogen, to relieve any short contacts. To use the UCH-L3 protein structure in the following docking simulations, the structures of UCH-L3 and Ub-VME complex were divided into their components.

4.3. Virtual screening

Virtual screening experiments were performed by UCSF DOCK 5.4.0[10] and GOLD 3.0.1 (CCDC, Cambridge, UK).[26] In the first screening by DOCK, the substrate-binding site was defined, by selecting ligand atom accessible spheres and describing molecular surfaces with the SPHERE_GENERATOR program in the DOCK suite. All spheres within 6 Å of root mean square deviation (RMSD) from every atom of the three C-terminal residues of energy-minimized ubiquitin were selected by the SPHERE_SELECTOR program in DOCK suite. A scoring function ($E_{int} = E_{vdw} + E_{elec}$) was used to estimate potential binding affinity. Following the first screening with rigid ligand conditions, 1780 compounds with binding energy scores of less than −30 kcal/mol were selected for a second screening by GOLD.

Using GOLD, the 1780 compounds were screened with 7–8 times speed-up settings; that is, the pre-defined genetic algorithm (GA) parameter settings to achieve calculation speed-up. The top-ranked 100 compounds were determined, then screened by default settings; the GA parameter settings for a slower calculation with greater ligand flexibility, but with a more accurate prediction. Ligand flexibility was turned on in both the 7–8 times speed-up settings and the default settings. Protein side chain flexibility was not turned on in any settings. The virtual tripeptide structure composed of three C-terminal residues of the energy-minimized ubiquitin was set as the reference ligand to define the ligand-binding site. All protein atoms within 5 Å of each ligand atom were used for defining the binding site. The solvent-accessible surfaces of the docking region were restricted by a cavity detection algorithm.[27] As a result, the binding site was composed of 174 active atoms (automatically selected by GOLD software). A method for defining the binding site with tripeptide yielded the best score among other methods using shorter or longer C-terminal peptide sequences of ubiquitin (data not shown). Ten docking solutions for each docked molecule were scored and the top three were saved for post-screening evaluations. Potential hydrogen bonds and van der Waals contacts were identified using Silver 1.0 (CCDC, Cambridge, UK).[28] Ligands predicted to be tight-binders by both DOCK and GOLD were applied to further in vitro experimental validation. All calculations were performed on seven Linux or Cygwin 2–3 GHz/Pentium IV CPU personal computers.

4.4. Statistical analysis

All statistical analysis was performed by GraphPad Prism 4 (GraphPad Software, Inc., San Diego, CA).[29]

4.5. Reagents

Human recombinant UCH-L3, ubiquitin-7-amido-4-methylcoumarin (Ub-AMC), and ubiquitin-aldehyde (Ub-H) were purchased from Boston Biochem, Inc. (Cambridge, MA). 4,5,6,7-Tetrachloroindan-1,3-dione (TCI) was purchased from Fisher Scientific International Inc. (Hampton, NH). Iodoacetamide was purchased from Sigma–Aldrich Corporation (St. Louis, MO). Compounds within ChemBridge CNS-Set (Supplier IDs given in parentheses) are as follows: compound **1**: 1-benzyl-3-hydroxy-4-(5-methyl-2-furoyl)-5-(3-pyridinyl)-1,5-dihydro-2*H*-pyrrol-2-one (7504601); compound **2**: 3-[4-methyl-5-({[3-(2-thienyl)-1,2,4-oxadiazol-5-yl]methyl}thio)-4*H*-1, 2,4-triazol-3-yl]-1*H*-indole (7950509); compound **3**: *N*-{4-[1-(2-furoyl)-5-(2-furyl)-4,5-dihydro-1*H*-pyrazol-3-yl]phenyl}methanesulfonamide (7977303); compound **4**: N^1-cyclopropyl-N^2-(4-methoxyphenyl)-N^2-[(4- methylphenyl)sulfonyl]glycinamide (6382507); compound **5**: *N*-{3-[1-acetyl-5-(2-thienyl)-4,5-dihydro-1*H*-pyrazol-3-yl]phenyl}ethanesulfonamide (7909542); compound **6**: 3-hydroxy-5-(4-methoxyphenyl)-1-(1,3,4-thiadiazol-2-yl)-4-(2-thienylcarbonyl)-1,5-dihydro-2*H*-pyrrol-2-one (6237842); compound **7**: 5-(4-fluorophenyl)-3-hydroxy-4-(5-methyl-2-furoyl)-1-(3-pyridinylmethyl)-1,5-dihydro-2*H*-pyrrol-2-one (6771097); compound **8**: N^1-cyclopropyl-N^2-[(4-methoxyphenyl)sulfonyl]-N^2-(4-methylphenyl)glycinamide (6699002); compound **9**: N^1-cyclopentyl-N^2-(3-methoxyphenyl)-N^2-(phenylsulfonyl)glycinamide (6187162); and compound **10**: 4-({[5-(2-furyl)-4-phenyl-4*H*-1,2,4-triazol-3-yl]thio}methyl)-1,3-thiazol-2-amine (9012750) were purchased from ChemBridge Corporation (San Diego, CA).

4.6. Enzymatic assay

UCH-L3 activity was assayed using modification of a technique described in previous studies.[22,30] The enzyme

reactions were carried out at a final volume of 205 μl on Costar 96-well black assay plates (part number 3915, Corning Inc., Corning, NY). Then, 5 μl of solution containing each compound (100% DMSO), or 5 μl of 100% DMSO as a negative control, was added to 100 μl of enzyme buffer solution (50 pM of UCH-L3, 20 mM Hepes [pH 7.8], 0.5 mM EDTA, 5 mM dithiothreitol [DTT], and 0.1 mg/ml ovalbumin) in each well. The solution was incubated for 30 min at room temperature. To start the enzyme reaction, 100 μl of substrate buffer solution (82 nM of ubiquitin-AMC, 20 mM Hepes [pH 7.8], 0.5 mM EDTA, 5 mM DTT, and 0.1 mg/ml ovalbumin) was added to each well. AMC fluorescence (excitation wavelength: 355 nm, emission wavelength: 460 nm) was subsequently measured 40 times every 3 s with a Wallac 1420 multi-label counter (Perkin-Elmer, Wellesley, MA).

4.7. K_m determination

Fifty microliters of enzyme buffer solution was added to each plate well. The solution was incubated for 30 min at room temperature. To start the enzyme reaction, 50 μl of substrate buffer solution (23.1, 46.3, 92.5, 185, 370, and 740 nM of ubiquitin-AMC; the concentrations of other components were as described previously) was added to each well. Fluorescence of AMC was measured 40 times every 3 s with the Wallac multi-label counter. Initial velocities (from 0 to 30 s) were used for K_m determination, using GraphPad Prism 4 software.[29]

4.8. Experimental IC_{50} determination

Five microliters of solution containing each compound (0.412 μM, 1.23, 3.70, 11.1, 20, 33.3, 50, 100, 300, and 700–850 μM) or 5 μl of 100% DMSO (as a negative control) diluted in 100 μl of enzyme buffer solution was added to each plate well. This solution was incubated for 30 min at room temperature. To start the enzyme reaction, 100 μl of substrate buffer solution was added to each well. Fluorescence of AMC was measured 40 times every 3 s with the Wallac multi-label counter. Initial velocities (from 0 to 30 s) were used for IC_{50} determination, using GraphPad Prism 4 software.[29]

4.9. Active site binding experiment

Modification of a technique described in previous studies was used to determine whether or not the compounds bind to the active site.[22] Five microliters of solution containing compound **1** (0 μM, 61.8 μM, 185 μM, 556 μM, and 1.67 mM) or 5 μl of 100% DMSO (as a negative control) diluted in 80 μl of enzyme buffer solution (UCH-L3: 1 nM) was added to each plate well. This solution was incubated for 30 min at room temperature. To start the enzyme reaction, 80 μl of substrate buffer solution (Ub-AMC: 1 μM) was added to each well, followed within 2 s by addition of 40 μl of iodoacetamide (108 mM) or water as a negative control. Fluorescence of AMC was measured 100 times every second using the Wallac multi-label counter. The percentage of active site survival $[(F_{saturated} - F_t)/(F_{saturated} - F_{t=0}) \times 100]$ was calculated.

Acknowledgments

This work was supported by Grants-in-Aid for Scientific Research from the Ministry of Health, Labour and Welfare of Japan, Grants-in-Aid for Scientific Research from the Ministry of Education, Culture, Sports, Science and Technology of Japan, a grant from the Program for Promotion of Fundamental Studies in Health Sciences of the National Institute of Biomedical Innovation, a grant from Japan Science and Technology Cooperation, and a grant from New Energy and Industrial Technology Development Organization. We thank Takashi Kaburagi for demonstrating how to set up the DOCK software.

References and notes

1. Ciechanover, A.; Schwartz, A. L. *Proc. Natl. Acad. Sci. U.S.A.* **1998**, *95*, 2727–2730.
2. Pickart, C. M.; Rose, I. A. *J. Biol. Chem.* **1985**, *260*, 7903–7910.
3. Waldmeier, P.; Bozyczko-Coyne, D.; Williams, M.; Vaught, J. L. *Biochem. Pharmacol.* **2006**, *72*, 1197–1206.
4. Aktas, O.; Waiczies, S.; Zipp, F. *J. Neuroimmunol.* **2007**, *184*, 17–26.
5. Miyoshi, Y.; Nakayama, S.; Torikoshi, Y.; Tanaka, S.; Ishihara, H.; Taguchi, T.; Tamaki, Y.; Noguchi, S. *Cancer Sci.* **2006**, *97*, 523–529.
6. Rolen, U.; Kobzeva, V.; Gasparjan, N.; Ovaa, H.; Winberg, G.; Kisseljov, F.; Masucci, M. G. *Mol. Carcinog.* **2006**, *45*, 260–269.
7. Kwon, J.; Wang, Y. L.; Setsuie, R.; Sekiguchi, S.; Sato, Y.; Sakurai, M.; Noda, M.; Aoki, S.; Yoshikawa, Y.; Wada, K. *Am. J. Pathol.* **2004**, *165*, 1367–1374.
8. Sano, Y.; Furuta, A.; Setsuie, R.; Kikuchi, H.; Wang, Y. L.; Sakurai, M.; Kwon, J.; Noda, M.; Wada, K. *Am. J. Pathol.* **2006**, *169*, 132–141.
9. Kuntz, I. D.; Blaney, J. M.; Oatley, S. J.; Langridge, R.; Ferrin, T. E. *J. Mol. Biol.* **1982**, *161*, 269–288.
10. Ewing, T. J.; Makino, S.; Skillman, A. G.; Kuntz, I. D. *J. Comput. Aided Mol. Des.* **2001**, *15*, 411–428.
11. FlexX, BioSolveIT GmbH, Sankt Augustin, Germany, <http://www.biosolveit.de/>.
12. Peng, H.; Huang, N.; Qi, J.; Xie, P.; Xu, C.; Wang, J.; Yang, C. *Bioorg. Med. Chem. Lett.* **2003**, *13*, 3693–3699.
13. McNally, V. A.; Gbaj, A.; Douglas, K. T.; Stratford, I. J.; Jaffar, M.; Freeman, S.; Bryce, R. A. *Bioorg. Med. Chem. Lett.* **2003**, *13*, 3705–3709.
14. Olsen, L.; Jost, S.; Adolph, H. W.; Pettersson, I.; Hemmingsen, L.; Jorgensen, F. S. *Bioorg. Med. Chem.* **2006**, *14*, 2627–2635.
15. Miteva, M. A.; Lee, W. H.; Montes, M. O.; Villoutreix, B. O. *J. Med. Chem.* **2005**, *48*, 6012–6022.
16. Johnston, S. C.; Larsen, C. N.; Cook, W. J.; Wilkinson, K. D.; Hill, C. P. *EMBO J.* **1997**, *16*, 3787–3796.
17. Misaghi, S.; Galardy, P. J.; Meester, W. J.; Ovaa, H.; Ploegh, H. L.; Gaudet, R. *J. Biol. Chem.* **2005**, *280*, 1512–1520.
18. RPBS, Paris, France, <http://bioserv.rpbs.jussieu.fr/RPBS/cgi-bin/Ressource.cgi?chzn_lg=an&chzn_rsrc=Collections/>.
19. GOLD User Guide, 16.2.1, CCDC, Cambridge, UK, <http://www.ccdc.cam.ac.uk/support/documentation/gold/3_1/gold31.pdf/>.
20. Dang, L. C.; Melandri, F. D.; Stein, R. L. *Biochemistry* **1998**, *37*, 1868–1879.

21. Mason, D. E.; Ek, J.; Peters, E. C.; Harris, J. L. *Biochemistry* **2004**, *43*, 6535–6544.
22. Liu, Y.; Lashuel, H. A.; Choi, S.; Xing, X.; Case, A.; Ni, J.; Yeh, L. A.; Cuny, G. D.; Stein, R. L.; Lansbury, P. T., Jr. *Chem. Biol.* **2003**, *10*, 837–846.
23. Stenlund, P.; Frostell-Karlsson, A.; Karlsson, O. P. *Anal. Biochem.* **2006**, *353*, 217–225.
24. Das, C.; Hoang, Q. Q.; Kreinbring, C. A.; Luchansky, S. J.; Meray, R. K.; Ray, S. S.; Lansbury, P. T.; Ringe, D.; Petsko, G. A. *Proc. Natl. Acad. Sci. U.S.A.* **2006**, *103*, 4675–4680.
25. Kurihara, L. J.; Semenova, E.; Levorse, J. M.; Tilghman, S. M. *Mol. Cell. Biol.* **2000**, *20*, 2498–2504.
26. Jones, G.; Willett, P.; Glen, R. C.; Leach, A. R.; Taylor, R. *J. Mol. Biol.* **1997**, *267*, 727–748.
27. Hendlich, M.; Rippmann, F.; Barnickel, G. *J. Mol. Graph. Model.* **1997**, *15*, 359–363.
28. Silver, CCDC, Cambridge, UK, <http://www.ccdc.cam.ac.uk/>.
29. GraphPad Prism 4, GraphPad Software, San Diego, CA, <http://www.graphpad.com/www/about.htm/>.
30. Nishikawa, K.; Li, H.; Kawamura, R.; Osaka, H.; Wang, Y. L.; Hara, Y.; Hirokawa, T.; Manago, Y.; Amano, T.; Noda, M.; Aoki, S.; Wada, K. *Biochem. Biophys. Res. Commun.* **2003**, *304*, 176–183.

Available online at www.sciencedirect.com
ScienceDirect
Neuroscience Research 60 (2008) 106–113
Neuroscience Research
www.elsevier.com/locate/neures

Preventing effects of a novel anti-parkinsonian agent zonisamide on dopamine quinone formation

Masato Asanuma [a,*], Ikuko Miyazaki [a], Francisco J. Diaz-Corrales [a], Ko Miyoshi [a], Norio Ogawa [a], Miho Murata [b]

[a] *Department of Brain Science, Okayama University Graduate School of Medicine, Dentistry and Pharmaceutical Sciences, 2-5-1 Shikatacho, Okayama 700-8558, Japan*
[b] *Department of Neurology, Musashi Hospital, National Center of Neurology and Psychiatry, Tokyo, Japan*

Received 10 August 2007; accepted 3 October 2007
Available online 10 October 2007

Abstract

The neurotoxicity of dopamine (DA) quinones as dopaminergic neuron-specific oxidative stress is considered to play a role in the pathogenesis and/or progression of Parkinson's disease (PD), since DA quinones conjugate with several key PD pathogenic molecules (*e.g.*, tyrosine hydroxylase, α-synuclein and parkin) to form protein-bound quinone (quinoprotein) and consequently inhibit their functions. Zonisamide (ZNS) is used as an anti-epileptic agent but also improved the cardinal symptoms of PD in recent clinical trials in Japan. To evaluate the effects of ZNS on excess cytosolic free DA-induced quinone toxicity, we examined changes in DA quinone-related indices after ZNS treatment both in *in vitro* cell-free system and in cultured cells. Co-incubation of DA and ZNS in a cell-free system caused conversion of DA to stable melanin via formation of DA-semiquinone radicals and DA chrome. Long-term (5 days) treatment with ZNS decreased quinoprotein and increased DA/DOPA chromes in dopaminergic CATH.a cells. ZNS significantly inhibited quinoprotein formation induced by treatment with tetrahydrobiopterin and ketanserin that elevate cytosolic free DA in the cells. Our results suggest that the novel anti-parkinsonian agent ZNS possesses preventing effects against DA quinone formation induced by excess amount of cytosolic DA outside the synaptic vesicles.

Keywords: Zonisamide; Dopamine chrome; Dopamine quinone; Quinoprotein; Parkinson's disease

1. Introduction

Under normal conditions, dopamine (DA) is stable in the synaptic vesicle. However, when levodopa is administered to the damaged dopaminergic neuronal system of Parkinson's disease (PD), a large amount of DA remains in the cytosol outside the synaptic vesicle, since the damaged dopaminergic system has too small DA pool to store DA (Sulzer et al., 2000; Sulzer and Zecca, 2000; Asanuma et al., 2003; Ogawa et al., 2005). The toxicity of excess levodopa and/or DA has been well documented in many *in vitro* and *in vivo* animal studies using parkinsonian models (Ogawa et al., 1993; Basma et al., 1995; Walkinshaw and Waters, 1995; Hastings et al., 1996; Asanuma et al., 2003), despite its marked beneficial effects. Free excess DA is easily metabolized via monoamine oxidase (MAO)-B or by auto-oxidation to produce cytotoxic reactive oxygen species (ROS), and then forms neuromelanin (Sulzer et al., 2000; Sulzer and Zecca, 2000). In the oxidation of DA by MAO, DA is converted to dihydroxyphenylacetic acid (DOPAC) to generate general ROS hydrogen peroxide. On the other hand, non-enzymatic and spontaneous auto-oxidation of DA and L-DOPA produces superoxide and reactive quinones such as DA quinones and DOPA quinones (Tse et al., 1976; Graham, 1978). DA quinones are also generated in the enzymatic oxidation of DA by prostaglandin H synthase (cyclooxygenase-2), lipoxygenase, tyrosinase and xanthine oxidase (Korytowski et al., 1987; Rosei et al., 1994; Hastings, 1995; Foppoli et al., 1997; Chae et al., 2007). These quinones are oxidized to the cyclized aminochromes: DA chrome (aminochrome) and DOPA chrome, and then are finally polymerized to form melanin. Although ROS generation by the auto-oxidation of DA may explain widespread

* Corresponding author. Tel.: +81 86 235 7408; fax: +81 86 235 7412.
E-mail address: asachan@cc.okayama-u.ac.jp (M. Asanuma).

0168-0102/$ – see front matter
doi:10.1016/j.neures.2007.10.002

toxicity but not specific damage of DA neurons, the highly reactive DA quinone or DOPA quinone itself exerts predominant cytotoxicity in DA neurons and surrounding neural cells, since these quinones are generated from free cytosolic DA outside the synaptic vesicle or from L-DOPA (Sulzer et al., 2000).

The generated DA quinones covalently conjugate with the sulfhydryl group of cysteine on functional proteins, resulting predominantly in the formation of 5-cysteinyl-DA (Graham, 1978; Fornstedt et al., 1986). DA quinones conjugate with cysteine residues of various functional proteins including several key molecules involved in the pathogenesis of PD (*e.g.*, tyrosine hydroxylase, DA transporter and parkin) to form protein-bound quinones (quinoproteins), and inhibit the function of these proteins to cause DA neuron-specific cytotoxicity (Xu et al., 1998; Kuhn et al., 1999; Whitehead et al., 2001; LaVoie et al., 2005; Machida et al., 2005). We reported previously that repeated levodopa administration elevated striatal DA turnover and formation of quinoproteins specifically in the parkinsonian side, but not in the control side, of hemi-parkinsonian models (Ogawa et al., 2000; Asanuma et al., 2005; Miyazaki et al., 2005). Therefore, the excess amount of cytosolic DA outside the synaptic vesicles after levodopa treatment may exert neurodegenerative effects through quinone generation, at least in the damaged dopaminergic nerve terminals. The DA-induced formation of DA quinones and the consequent dopaminergic cell damage *in vitro* and *in vivo* could be prevented by treatment with superoxide dismutase, glutathione, and certain thiol reagents through their quinone-quenching activities (Offen et al., 1996; Lai and Yu, 1997; Kuhn et al., 1999; Haque et al., 2003). We also demonstrated recently that DA agonists pergolide and pramipexole exhibit quenching properties against *in vitro* generated DA-semiquinone radicals (Asanuma et al., 2005; Miyazaki et al., 2005), and that pergolide effectively prevented repeated levodopa-induced elevation of striatal quinoprotein specifically in parkinsonian models (Miyazaki et al., 2005). Thus, DA quinones act as neurotoxic compounds by eliciting dopaminergic neuron-specific oxidative stress and thus play a role in the pathogenesis and/or progression of PD and neurotoxin-induced parkinsonism (Choi et al., 2003, 2005; Asanuma et al., 2004; LaVoie et al., 2005; Machida et al., 2005; Ogawa et al., 2005; Chae et al., 2007).

Zonisamide (1,2-benzisoxazole-3-methaesulfonamide: ZNS), which was originally synthesized in Japan, has been used as an anti-epileptic agent in Japan, South Korea, USA and Europe. An open trial of ZNS (50–200 mg/day) administered in conjunction with anti-PD drugs showed lessening of symptoms, especially wearing-off (Murata et al., 2001), and induced more than 30% improvement of UPDRS total score up to 3 years (Murata, 2004). The addition of ZNS to levodopa treatment of patients experiencing 'wearing-off' fluctuations resulted in lessening of motor fluctuation and significant improvement of the duration, severity and activities of daily living in 'off' time and score of motor examination. Furthermore, a recent nationwide double-blind controlled study in Japan reported that an adjunctive treatment with lower dose of ZNS (25–100 mg/day) to levodopa improved all the cardinal symptoms of PD (Murata, 2004; Murata et al., 2007).

Several pharmacological effects of ZNS have been proposed to be related to its beneficial effects on PD. ZNS is a specific T-type Ca^{++} channel blocker (Suzuki et al., 1992; Kito et al., 1996), which increases burst firing of dopaminergic neurons in the substantia nigra. A single dose of ZNS increased intracellular and extracellular DOPA, DA and homovanillic acid (HVA) levels and decreased DOPAC level in the rat striatum presumably through its moderate MAO-inhibiting effect (Okada et al., 1992, 1995). Long-term administration of ZNS increased activity and protein level of tyrosine hydroxylase in the rat striatum (Murata, 2004), and thus enhanced DA synthesis. However, these effects cannot fully explain the mechanism of its therapeutic effects on levodopa-induced adverse effects.

To evaluate the effects of ZNS on excess cytosolic free DA-induced quinone toxicity, we examined changes in DA quinone-related indices after ZNS treatment both in *in vitro* cell-free DA-semiquinone generating system and in cultured dopaminergic neuronal cells.

2. Materials and methods

2.1. Materials

DA hydrochloride and L-DOPA were purchased from Wako Pure Chemical (Tokyo, Japan) and Sigma (St. Louis, MO), respectively. ZNS and its sodium salt were provided by Dainippon Sumitomo Pharma (Osaka, Japan).

2.2. ESR spectrometry of generated DA-semiquinone radicals

The spectra of semiquinone radicals generated from DA in a cell-free system were recorded with an electron spin resonance (ESR) spectrometer (JES-FR30, JEOL Co., Tokyo) using a flat quartz cuvette as reported previously (Korytowski et al., 1987; Haque et al., 2003). DA or L-DOPA was dissolved in 10 mM sodium phosphate buffer (PB: pH 7.4), and the pH was adjusted to 7.0 by adding 0.1 M NaOH at 4 °C. For the experiment on time-dependency, the pH-adjusted DA or L-DOPA (final concentration 1 mM) was immediately incubated with ZNS sodium salt dissolved in 10 mM PB (final concentration 8 mM, pH 10.8) for 1–60 min at 37 °C, and the spectra for these combinations were analyzed. As a positive control to generate DA-semiquinone, tyrosinase (final concentration 12.5 μg/ml) was incubated instead of ZNS. Furthermore, 0.1 N NaOH (pH 10.9) or pH-adjusted 10 mM PB (pH 10.8) was used instead of ZNS as a negative control. For the experiment on dose-dependency, the pH-adjusted DA (final concentration 1 mM, pH 7.0), with or without various concentrations (ranging from 2 to 8 mM) of ZNS sodium salt dissolved in 10 mM PB (pH 10.8), was immediately incubated for 1 min at 37 °C, and the spectra for these combinations were analyzed. The pH of each final incubation mixture was approximately 8.0. The signal intensity was evaluated by the relative peak height of the second signal of the semiquinone radical spin adduct (the peak height of the second signal is higher than the others and is directly proportional to double integration of the spectra) to the intensity of the Mn^{2+} signal, which was used as the internal standard to correct for measurement error. The conditions of the ESR spectrometer to estimate the semiquinone radical, including magnetic field, power, modulation frequency, modulation amplitude, response time, temperature, amplitude, and sweep time were 335 ± 5 mT, 4 mW, 9.41 GHz, 79 μT, 0.1 s, 25 °C, 1 × 1000 and 1 min, respectively. Furthermore, the levels of DA and its metabolites in the reaction mixture were measured by high-performance liquid chromatography (HPLC) as described previously (Ogawa et al., 2000; Asanuma et al., 2005).

2.3. Effects of ZNS on generation of DA chrome

To examine the effects of ZNS on generation of DA chrome in a cell-free system, pH-adjusted 1 mM DA in 10 mM PB (pH 6.8) and 0.2% Triton X-100 solution were incubated with or without 200 μM ZNS dissolved in 10 mM PB (pH 6.8) for 1 min to 3 h at 37 °C. The level of DA chrome in the final mixture (pH 6.8) was estimated by measuring absorbance of incubation mixture at 475 nm.

2.4. Cell culture and drug treatment

Dopaminergic CATH.a cells (ATCC; #CRL-11179), derived from mouse DA-containing neurons, were cultured at 37 °C in 5% CO_2 in RPMI 1640 culture medium (Invitrogen, San Diego, CA) supplemented with 4% fetal bovine serum, 8% horse serum, 100 U/ml penicillin and 100 μg/ml streptomycin. Cells were seeded in 6-well plates (Becton Dickinson Labware, Franklin Lakes, NJ) for the extraction of cell lysates used for the measurement of protein-bound quinone and DA/DOPA chrome at a density of 1.0×10^5 cells/cm^2. After 24 h, CATH.a cells were exposed to 1–100 μM ZNS diluted in phosphate buffered saline (PBS) for 5 days for the measurements of quinoprotein and DA/DOPA chrome. To examine the effects of ZNS on excess cytosolic free DA-induced quinone elevation, CATH.a cells were exposed simultaneously to 1–100 μM ZNS with 100 μM tetrahydrobiopterin (BH_4) and 10 μM ketanserin, which enhance DA synthesis and blocks vesicle monoamine transporter, respectively (Choi et al., 2005), for 3 h before extraction of total cell lysates for quinoprotein measurement.

2.5. Protein-bound quinone; quinoprotein measurement

Total cell lysates from drug-treated CATH.a cells were prepared with 10 μg/ml phenylmethylsulfonyl fluoride (Sigma) in ice cold-RIPA buffer [PBS (pH 7.4), 1% nonidet P-40 (NP-40), 0.5% sodium deoxycholate and 0.1% sodium dodecyl sulfate]. The nitrobluetetrazolium (NBT)/glycinate colorimetric assay was performed to detect protein-bound quinones (quinoprotein) (Paz et al., 1991). The cell lysate was added to 500 μl of NBT reagent (0.24 mM NBT in 2 M potassium glycinate, pH 10.0) followed by incubation in the dark for 2 h under constant shaking. The absorbance of blue-purple color developed in the reaction mixture was measured at 530 nm.

2.6. Measurement of DA/DOPA chrome in CATH.a cells

For the measurement of DA/DOPA chrome, cells were solubilized in 500 μl of 1% Triton X-100 solution for 2 h and then centrifuged at 20,000 × *g* for 30 min at 4 °C. The supernatant was used as cell extract and incubated for 3 min at room temperature. The level of DA/DOPA chrome was calculated by measuring absorbance of incubated cell extract at 475 nm. Absorbance values in the *in vitro* incubation of DA (0–500 μM) with tyrosinase (10 μg/ml) for 30 min were used as a standard to calculate the concentration of DA/DOPA chrome in the cell extract.

2.7. Protein measurement

The protein concentration was determined using the Bio-Rad protein assay kit or Bio-Rad DC protein assay kit (Bio-Rad, Richmond, CA), based on the method of Bradford and Lowry, respectively, using bovine serum albumin as a standard.

2.8. Statistical analysis

Results are expressed as mean ± S.E.M. values. Statistical analysis of the data was performed using one-way ANOVA followed by *post hoc* Fisher's PLSD test. A *p*-value less than 0.05 denoted the presence of a statistically significant difference.

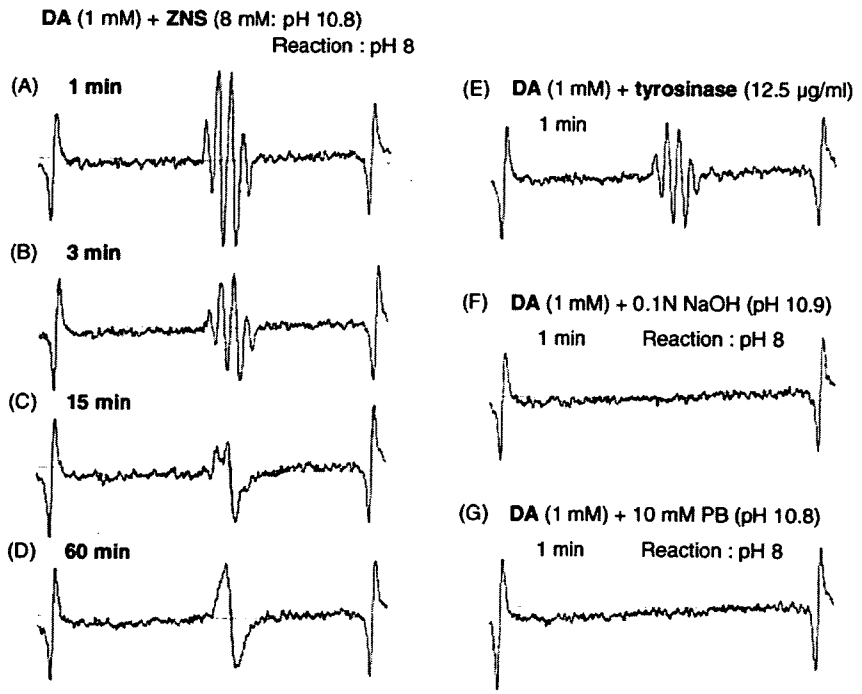

Fig. 1. Effects of ZNS on DA-semiquinone radicals generated from DA in a cell-free system. (A–D) Representative time-course changes in ESR spectra of DA-semiquinone radicals (A–B) to melanin (D) in the incubation of pH-adjusted 1 mM DA (pH 7.0) with 8 mM ZNS (sodium salt) in 10 mM PB (pH 10.8) for 1–60 min at 37 °C at pH 8.0 (incubation mixture). (E) Formation of DA-semiquinone radicals via tyrosinase (12.5 μg/ml)-catalyzed oxidation of 1 mM DA. (F and G) No signals for radical formation at pH 8.0 (incubation mixture) when pH-adjusted 1 mM DA (pH 7.0) was incubated for 1 min at 37 °C with 0.1 N NaOH (pH 10.9) (F) or pH-adjusted 10 mM PB (pH 10.8) (G). Each experiment was performed as triplicate assays.

3. Results

3.1. Effects of ZNS on generated DA-semiquinone radicals in a cell-free system

When a high dose of DA (5 mM) was incubated at 37 °C at neutral pH 7–8, the formation of DA-semiquinone radicals started immediately within 1 min, peaked at around 1 min, then gradually decreased and continued for 10 min, as shown in a previous study (Haque et al., 2003). In the present ESR study, however, no signals for radical formation were detected at pH 8 (incubation mixture) when a lower dose of pH-adjusted 1 mM DA (pH 7.0) was incubated for 1 min at 37 °C with 0.1 N NaOH (pH 10.9) or pH-adjusted 10 mM PB (pH 10.8) (Fig. 1F and G). Interestingly, when pH-adjusted 1 mM DA (pH 7.0) was incubated at 37 °C with 8 mM ZNS (sodium salt) in 10 mM PB (pH 10.8), the formation of DA-semiquinone radicals, which was identified by four waves in ESR spectrometry, started immediately within 1 min and peaked at around 1 min, at pH 8 (incubation mixture) (Fig. 1A and B), as well as formation of DA-semiquinone radicals via tyrosinase-catalyzed oxidation of DA (Fig. 1E). Then, the DA-semiquinone radical induced by incubation of DA and ZNS converted to melanin, which was recognized by a wide single wave, at 15–60 min (Fig. 1C and D). The incubation of pH-adjusted 1 mM DA (pH 7.0) and 2–8 mM ZNS (sodium salt, pH 10.8) at pH 8 (incubation mixture) resulted in DA-semiquinone radical formation at 1 min (Fig. 2A–D) and subsequent melanin formation at 60 min (data not shown) in a ZNS concentration-dependent manner. Furthermore, incubation of pH-adjusted 1 mM L-DOPA (pH 7.0) with 8 mM ZNS (sodium salt, pH 10.8) at 37 °C at pH 8 (incubation mixture) resulted in immediate generation of DOPA-semiquinone radicals within 1 min, with a peak at around 1 min, and conversion to melanin within up to 20 min (Fig. 2E–G). DOPAC, 3-methoxy tyramine and HVA, which are metabolites of DA via MAO and/or catecholamine *o*-methyltransferase, were not detected in any incubation mixture of pH-adjusted DA and ZNS (sodium salt) at either dose of ZNS or incubation time by HPLC (data not shown).

3.2. Effects of ZNS on generation of DA chrome in a cell-free system

Because a high dose of ZNS was required to detect the conversion effects from DA to melanin in ESR spectrometry, we used sodium salt of ZNS, which is highly soluble in 10 mM PB, at a dose of 2–8 mM. However, the pH value of the mixture of ESR examination was slightly alkaline at 8.0 because of high alkalinity of ZNS sodium salt solution (pH 10.8) in the cell-free system. To examine the effects of relatively low dose of ZNS on conversion of DA to melanin at neutral pH, we evaluated generation of DA chrome, which is an intermediate in conversion of DA quinone to melanin, using 200 μM ZNS at pH 6.8, but not its sodium salt (Fig. 3). Although the incubation of pH-adjusted 1 mM DA (pH 6.8) alone at 37 °C showed time-dependent but not significant increases in DA

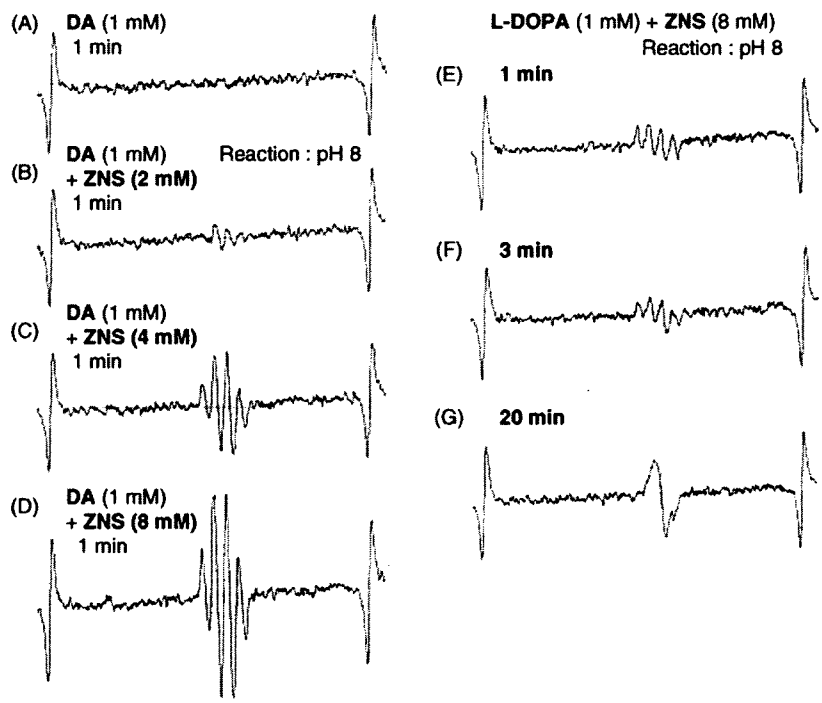

Fig. 2. Effects of ZNS on semiquinone radicals generated from DA or L-DOPA. (A–D) Dose-dependent effects of ZNS on DA-semiquinone radicals generated from DA in a cell-free system. The pH-adjusted 1 mM DA (pH 7.0) was simultaneously incubated with 2–8 mM ZNS (pH 10.8) at pH 8.0 (incubation mixture) for 1 min at 37 °C, and then the relative signal intensity of DA-semiquinone radicals was measured by ESR spectrometry. (E–G) Representative time-course changes in ESR spectra of DOPA-semiquinone radicals (E and F) to melanin (G) in the incubation of pH-adjusted L-DOPA (1 mM, pH 7.0) with 8 mM ZNS (sodium salt) in 10 mM PB (pH 10.8) for 1–20 min at 37 °C at pH 8.0 (incubation mixture). Three independent assays were performed in each experiment.

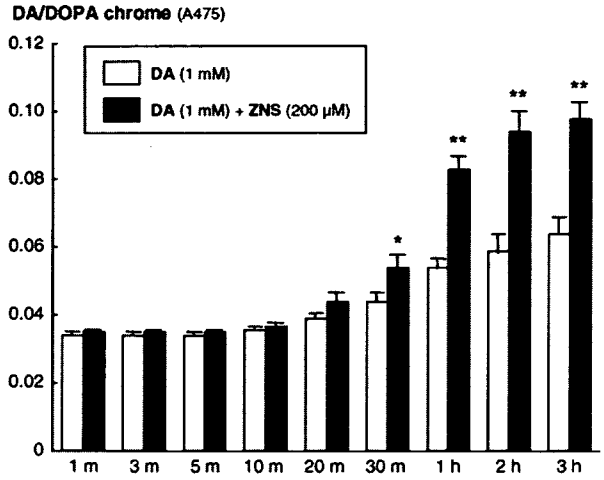

Fig. 3. Effects of ZNS on time-course changes in DA/DOPA chrome generated in a cell-free system. Levels of generated DA/DOPA chrome were measured after incubation of pH-adjusted 1 mM DA (pH 6.8) with/without 200 μM ZNS (pH 6.8) at 37 °C for 1 min to 3 h. Co-incubation of pH-adjusted DA (1 mM) and ZNS (200 μM) at neutral pH significantly increased DA/DOPA chrome at 30 min to 3 h, compared with time-matched pH-adjusted DA alone. Each value is the mean of absorbance at 475 nm ± S.E.M. ($n = 5$). *$p < 0.05$, **$p < 0.001$ compared with time-matched group treated with DA alone.

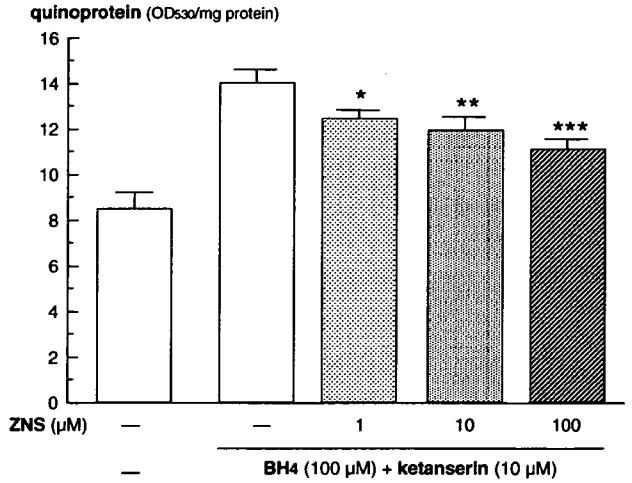

Fig. 5. Effects of ZNS treatment on excess cytosolic free DA-induced quinoprotein formation in dopaminergic CATH.a cells. Quinoprotein level in CATH.a cells were measured after treatment with BH_4 (100 μM) and ketanserin (10 μM), with or without ZNS (1–100 μM) for 3 h. The simultaneous treatment of ZNS (1–100 μM) significantly and dose-dependently inhibited BH_4 plus ketanserin-induced quinoprotein formation. Data are mean ± S.E.M. ($n = 8$). *$p < 0.05$, **$p < 0.01$ and ***$p < 0.001$ compared with cells treated with BH_4 plus ketanserin without ZNS.

chrome level, co-incubation of pH-adjusted 1 mM DA (pH 6.8) and 200 μM ZNS (pH 6.8) at 37 °C significantly increased DA chrome at 30 min to 3 h, compared with time-matched pH-adjusted DA alone.

3.3. Effects of ZNS on DA quinone formation in CATH.a cells

We examined changes in DA, its metabolites, quinoprotein and DA/DOPA chrome using *in vitro* dopaminergic CATH.a cells after 5-day treatment of ZNS. Quinoprotein level was significantly decreased after 5-day treatment of ZNS (10–100 μM) (Fig. 4) with reduction of DOPAC level (data not shown). On the other hand, 5-day treatment of ZNS (1–100 μM) significantly increased DA/DOPA chrome level in CATH.a cells (Fig. 4).

Finally, we examined the effects of ZNS on excess cytosolic free DA-induced quinone formation by measuring quinoprotein levels in CATH.a cells after treatment with BH_4 (100 μM) and ketanserin (10 μM) with/without ZNS (1–100 μM) for 3 h. The quinoprotein levels in CATH.a cells co-treated with BH_4 and ketanserin for 3 h (which increase cytosolic free DA) were relatively higher than that in control at day 1 (Fig. 5), in agreement with a previous report (Choi et al., 2005). The simultaneous treatment of ZNS (1–100 μM) significantly and dose-dependently inhibited BH_4- and ketanserin-induced quinoprotein formation in the cells (Fig. 5).

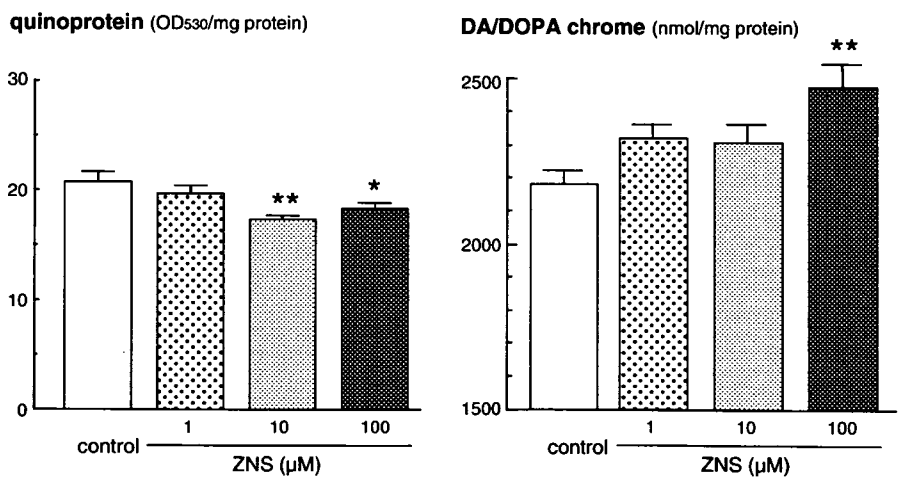

Fig. 4. Effects of long-term treatment of ZNS on quinoprotein and DA/DOPA chrome in dopaminergic CATH.a cells. After treatment with ZNS (1–100 μM) for 5 days, levels of quinoprotein ($n = 5$) and DA/DOPA chrome ($n = 6$) were measured in dopaminergic CATH.a cells, as indicated in Section 2. Data are mean ± S.E.M. *$p < 0.05$, **$p < 0.01$ compared with the control group.

4. Discussion

The main findings of this study are: (1) co-incubation of DA and ZNS in a cell-free system caused conversion of DA to stable melanin via formation of DA-semiquinone radicals and DA chrome; (2) long-term treatment with ZNS for 5 days decreased quinoprotein and increased DA/DOPA chromes in dopaminergic CATH.a cells; and (3) ZNS significantly inhibited quinoprotein formation induced by BH_4 and ketanserin that increase cytosolic free DA in the cells.

Long-term treatment of patients with PD by levodopa frequently causes various adverse effects including the wearing-off phenomenon, dyskinesia and psychiatric symptoms (Ahlskog and Muenter, 2001; Ogawa et al., 2005). However, long-term levodopa treatment-induced adverse effects that might be based on permanent neuronal network remodeling were seen specifically in PD patients but not in normal subjects or neurological diseases other than PD (Ogawa et al., 2005). Since the striatal damaged nerve terminal have too small DA pool to store DA at advanced stage of PD, repeated intermittent pulsatile levodopa stimulation results in free DA excess in the cytosol outside the synaptic vesicle (Sulzer et al., 2000; Sulzer and Zecca, 2000; Asanuma et al., 2003; Ogawa et al., 2005). The previous study revealed that repeated levodopa administration elevated striatal quinoprotein levels specifically on the parkinsonian side, not on the control side, of hemi-parkinsonian mice (Miyazaki et al., 2005). Therefore, the parkinsonian side-specific elevation of quinone generation may be due to excess amount of cytosolic DA outside the synaptic vesicles, which is easily oxidized to DA quinones in damaged dopaminergic nerve terminals after repeated levodopa treatment. In cultured dopaminergic cells, simultaneous treatment with ZNS dose-dependently suppressed BH_4- and ketanserin-induced quinoprotein formation via elevation of cytosolic free DA (Fig. 5), suggesting that ZNS has potent neuroprotective effects against neurotoxicity of DA quinone induced by excess amount of cytosolic DA outside the synaptic vesicles.

The protective effects of ZNS against levodopa-induced DA quinone toxicity in parkinsonian models may be based, in part, on its stabilizing effects against free DA and cytotoxic DA quinone; ZNS can convert free DA to melanin via the formation of DA-semiquinone radicals (Figs. 1 and 2) and subsequent intermediate DA chrome in the cell-free system (Fig. 3). This possible mechanism is also supported by the present results of long-term treatment with ZNS in cultured dopaminergic CATH.a cells. Long-term ZNS treatment in CATH.a cells for 5 days significantly decreased quinoprotein and increased DA/DOPA chromes (Fig. 4) with reduction of DOPAC (data not shown), suggesting that continuous ZNS exposure to DA-rich CATH.a cells promotes conversion of free DA and DA quinone to DA chrome, then to melanin. However, these effects do not seem to be exerted in a dose-dependent manner. Likewise relatively low doses of ZNS (25, 50 mg/day) rather than 100 mg/day significantly improved UPDRS Part III total score in the clinical trial (Murata et al., 2007), there may be optimal concentration range of ZNS to exert its stabilizing effects against DA quinones.

Several neuroprotective strategies have been proposed against DA quinone-induced cytotoxicity: (1) quenching excess free DA and DA quinone, (2) inhibiting quinone formation, and (3) enhancing intrinsic antioxidative system against DA quinone toxicity (Asanuma et al., 2004). Regarding quenching DA quinone, DA quinone can be scavenged by direct conjugation with some drugs, *e.g.*, thiol-containing compounds (*N*-acetylcyteine and dithiothreitol) (Offen et al., 1996) and DA agonists (pergolide and pramipexole) (Asanuma et al., 2005; Miyazaki et al., 2005). Furthermore, another possible method to quench DA quinone-induced cytotoxicity is the conversion of free DA and DA quinone to stable melanin. The final oxidized form of DA quinone, neuromelanin, exerts cytoprotective effects through its binding capacity to toxic metals (Zecca et al., 2003). Although large amount of neuromelanin with iron is reported to be potentially cytotoxic, physiological amount of neuromelanin is not toxic and rather cytoprotective with its high storage capacity for toxic metals in the substantia nigra (Gerlach et al., 2003; Zecca et al., 2003). This cytoprotective potency by stabilization of DA quinone has been clarified by our previous report that melanin-synthesizing enzyme tyrosinase ameliorates methamphetamine-induced neurotoxicity and quinoprotein formation *in vitro* and *in vivo* by its rapid conversion of DA quinone to melanin (Miyazaki et al., 2006). Also in the present study, we showed that ZNS can convert free DA to melanin via the formation of DA quinone and the intermediate DA chrome in the cell-free system. Therefore, these stabilizing effects of ZNS on free DA and DA quinone by the conversion to melanin may be one of the plausible mechanisms of its prevention against DA quinone-induced cytotoxicity.

ZNS is also known to scavenge hydroxyl radicals and nitric oxide radicals in a cell-free system (Mori et al., 1998) and inhibits lipid peroxidation and oxidative DNA damage in the rat brain (Komatsu et al., 2000). The general ROS such as hydroxyl radicals and nitric oxide radicals show widespread toxicity not only in DA neurons but also in other regions. Since the DA quinone is specifically generated from free cytosolic DA (Sulzer et al., 2000), the stabilizing effects of ZNS on free DA and cytotoxic DA quinone as dopaminergic neuron-specific oxidative stress may play a role in its preventing property against DA or levodopa-induced DA quinone toxicity, in addition to its scavenging activity against general ROS.

In conclusion, ZNS suppressed excess cytosolic free DA-induced quinone generation in dopaminergic cells. Furthermore, ZNS stabilized free DA and DA quinone as dopaminergic neuron-specific oxidative stress by the conversion to melanin. The stabilizing effects of ZNS against cytotoxic DA quinones may play a role in the efficacy of its adjunctive treatment to levodopa in parkinsonian patients.

Acknowledgments

This work was supported in part by Health and Labour Sciences Research Grants for Research on Measures for Intractable Diseases, for Research on Psychiatric and Neuro-

logical Diseases and Mental Health, and for Comprehensive Research on Aging and Health from the Japanese Ministry of Health, Labour and Welfare, and by Grants-in-Aid for Young Scientists (B) and for Scientific Research (C) from the Japanese Ministry of Education, Culture, Sports, Science and Technology. We would like to thank Mr. Yusuke Urakubo, Mr. Yasutsugu Tsutsui, and Mr. Masashi Yoshimoto for their technical assistance.

References

Ahlskog, J.E., Muenter, M.D., 2001. Frequency of levodopa-related dyskinesias and motor fluctuations as estimated from the cumulative literature. Mov. Disord. 16, 448–458.

Asanuma, M., Miyazaki, I., Diaz-Corrales, F.J., Ogawa, N., 2004. Quinone formation as dopaminergic neuron-specific oxidative stress in pathogenesis of sporadic Parkinson's disease and neurotoxin-induced parkinsonism. Acta Med. Okayama 58, 221–233.

Asanuma, M., Miyazaki, I., Diaz-Corrales, F.J., Shimizu, M., Tanaka, K., Ogawa, N., 2005. Pramipexole has ameliorating effects on levodopa-induced abnormal dopamine turnover in parkinsonian striatum and quenching effects on dopamine-semiquinone generated *in vitro*. Neurol. Res. 27, 533–539.

Asanuma, M., Miyazaki, I., Ogawa, N., 2003. Dopamine- or L-DOPA-induced neurotoxicity: the role of dopamine quinone formation and tyrosinase in a model of Parkinson's disease. Neurotox. Res. 5, 165–176.

Basma, A.N., Morris, E.J., Nicklas, W.J., Geller, H.M., 1995. L-dopa cytotoxicity to PC12 cells in culture is via its autoxidation. J. Neurochem. 64, 825–832.

Chae, S.W., Bang, Y.J., Kim, K.M., Lee, K.Y., Kang, B.Y., Kim, E.M., Inoue, H., Hwang, O., Choi, H.J., 2007. Role of cyclooxygenase-2 in tetrahydrobiopterin-induced dopamine oxidation. Biochem. Biophys. Res. Commun. 359, 735–741.

Choi, H.J., Kim, S.W., Lee, S.Y., Hwang, O., 2003. Dopamine-dependent cytotoxicity of tetrahydrobiopterin: a possible mechanism for selective neurodegeneration in Parkinson's disease. J. Neurochem. 86, 143–152.

Choi, H.J., Lee, S.Y., Cho, Y., Hwang, O., 2005. Inhibition of vesicular monoamine transporter enhances vulnerability of dopaminergic cells: relevance to Parkinson's disease. Neurochem. Int. 46, 329–335.

Foppoli, C., Coccia, R., Cini, C., Rosei, M.A., 1997. Catecholamines oxidation by xanthine oxidase. Biochim. Biophys. Acta 1334, 200–206.

Fornstedt, B., Rosengren, E., Carlsson, A., 1986. Occurrence and distribution of 5-*S*-cysteinyl derivatives of dopamine, dopa and dopac in the brains of eight mammalian species. Neuropharmacology 25, 451–454.

Gerlach, M., Double, K.L., Ben-Shachar, D., Zecca, L., Youdim, M.B., Riederer, P., 2003. Neuromelanin and its interaction with iron as a potential risk factor for dopaminergic neurodegeneration underlying Parkinson's disease. Neurotox. Res. 5, 35–44.

Graham, D.G., 1978. Oxidative pathways for catecholamines in the genesis of neuromelanin and cytotoxic quinones. Mol. Pharmacol. 14, 633–643.

Haque, M.E., Asanuma, M., Higashi, Y., Miyazaki, I., Tanaka, K., Ogawa, N., 2003. Apoptosis-inducing neurotoxicity of dopamine and its metabolites via reactive quinone generation in neuroblastoma cells. Biochim. Biophys. Acta 1619, 39–52.

Hastings, T.G., 1995. Enzymatic oxidation of dopamine: the role of prostaglandin H synthase. J. Neurochem. 64, 919–924.

Hastings, T.G., Lewis, D.A., Zigmond, M.J., 1996. Role of oxidation in the neurotoxic effects of intrastriatal dopamine injections. Proc. Natl. Acad. Sci. U.S.A. 93, 1956–1961.

Kito, M., Maehara, M., Watanabe, K., 1996. Mechanisms of T-type calcium channel blockade by zonisamide. Seizure 5, 115–119.

Komatsu, M., Hiramatsu, M., Willmore, L.J., 2000. Zonisamide reduces the increase in 8-hydroxy-2'-deoxyguanosine levels formed during iron-induced epileptogenesis in the brains of rats. Epilepsia 41, 1091–1094.

Korytowski, W., Sarna, T., Kalyanaraman, B., Sealy, R.C., 1987. Tyrosinase-catalyzed oxidation of dopa and related catechol(amine)s: a kinetic electron spin resonance investigation using spin-stabilization and spin label oximetry. Biochim. Biophys. Acta 924, 383–392.

Kuhn, D.M., Arthur Jr., R.E., Thomas, D.M., Elferink, L.A., 1999. Tyrosine hydroxylase is inactivated by catechol-quinones and converted to a redox-cycling quinoprotein: possible relevance to Parkinson's disease. J. Neurochem. 73, 1309–1317.

Lai, C.T., Yu, P.H., 1997. Dopamine- and L-β-3,4-dihydroxyphenylalanine hydrochloride (L-Dopa)-induced cytotoxicity towards catecholaminergic neuroblastoma SH-SY5Y cells. Effects of oxidative stress and antioxidative factors. Biochem. Pharmacol. 53, 363–372.

LaVoie, M.J., Ostaszewski, B.L., Weihofen, A., Schlossmacher, M.G., Selkoe, D.J., 2005. Dopamine covalently modifies and functionally inactivates parkin. Nat. Med. 11, 1214–1221.

Machida, Y., Chiba, T., Takayanagi, A., Tanaka, Y., Asanuma, M., Ogawa, N., Koyama, A., Iwatsubo, T., Ito, S., Jansen, P.H., Shimizu, N., Tanaka, K., Mizuno, Y., Hattori, N., 2005. Common anti-apoptotic roles of parkin and alpha-synuclein in human dopaminergic cells. Biochem. Biophys. Res. Commun. 332, 233–240.

Miyazaki, I., Asanuma, M., Diaz-Corrales, F.J., Fukuda, M., Kitaichi, K., Miyoshi, K., Ogawa, N., 2006. Methamphetamine-induced dopaminergic neurotoxicity is regulated by quinone formation-related molecules. FASEB J. 20, 571–573.

Miyazaki, I., Asanuma, M., Diaz-Corrales, F.J., Miyoshi, K., Ogawa, N., 2005. Dopamine agonist pergolide prevents levodopa-induced quinoprotein formation in parkinsonian striatum and shows quenching effects on dopamine-semiquinone generated *in vitro*. Clin. Neuropharmacol. 28, 155–160.

Mori, A., Noda, Y., Packer, L., 1998. The anticonvulsant zonisamide scavenges free radicals. Epilepsy Res. 30, 153–158.

Murata, M., 2004. Novel therapeutic effects of the anti-convulsant, zonisamide, on Parkinson's disease. Curr. Pharm. Des. 10, 687–693.

Murata, M., et al., 2007. Zonisamide improves motor function in Parkinson disease: a randomized, double-blind study. Neurology 68, 45–50.

Murata, M., Horiuchi, E., Kanazawa, I., 2001. Zonisamide has beneficial effects on Parkinson's disease patients. Neurosci. Res. 41, 397–399.

Offen, D., Ziv, I., Sternin, H., Melamed, E., Hochman, A., 1996. Prevention of dopamine-induced cell death by thiol antioxidants: possible implications for treatment of Parkinson's disease. Exp. Neurol. 141, 32–39.

Ogawa, N., Asanuma, M., Miyazaki, I., Diaz-Corrales, F.J., Miyoshi, K., 2005. L-DOPA treatment from the viewpoint of neuroprotection: possible mechanism of specific and progressive dopaminergic neuronal death in Parkinson's disease. J. Neurol. 252 (Suppl. 4), iv23–iv31.

Ogawa, N., Edamatsu, R., Mizukawa, K., Asanuma, M., Kohno, M., Mori, A., 1993. Degeneration of dopaminergic neurons and free radicals. Possible participation of levodopa. Adv. Neurol. 60, 242–250.

Ogawa, N., Tanaka, K., Asanuma, M., 2000. Bromocriptine markedly suppress levodopa-induced abnormal increase of dopamine turnover in the parkinsonian striatum. Neurochem. Res. 25, 755–758.

Okada, M., Kaneko, S., Hirano, T., Ishida, M., Kondo, T., Otani, K., Fukushima, Y., 1992. Effects of zonisamide on extracellular levels of monoamine and its metabolite, and on Ca^{2+} dependent dopamine release. Epilepsy Res. 13, 113–119.

Okada, M., Kaneko, S., Hirano, T., Mizuno, K., Kondo, T., Otani, K., Fukushima, Y., 1995. Effects of zonisamide on dopaminergic system. Epilepsy Res. 22, 193–205.

Paz, M.A., Fluckiger, R., Boak, A., Kagan, H.M., Gallop, P.M., 1991. Specific detection of quinoproteins by redox-cycling staining. J. Biol. Chem. 266, 689–692.

Rosei, M.A., Blarzino, C., Foppoli, C., Mosca, L., Coccia, R., 1994. Lipoxygenase-catalyzed oxidation of catecholamines. Biochem. Biophys. Res. Commun. 200, 344–350.

Sulzer, D., Bogulavsky, J., Larsen, K.E., Behr, G., Karatekin, E., Kleinman, M.H., Turro, N., Krantz, D., Edwards, R.H., Greene, L.A., Zecca, L., 2000. Neuromelanin biosynthesis is driven by excess cytosolic catecholamines not accumulated by synaptic vesicles. Proc. Natl. Acad. Sci. U.S.A. 97, 11869–11874.

Sulzer, D., Zecca, L., 2000. Intraneuronal dopamine-quinone synthesis: a review. Neurotox. Res. 1, 181–195.

Suzuki, S., Kawakami, K., Nishimura, S., Watanabe, Y., Yagi, K., Seino, M., Miyamoto, K., 1992. Zonisamide blocks T-type calcium channel in cultured neurons of rat cerebral cortex. Epilepsy Res. 12, 21–27.

Tse, D.C., McCreery, R.L., Adams, R.N., 1976. Potential oxidative pathways of brain catecholamines. J. Med. Chem. 19, 37–40.

Walkinshaw, G., Waters, C.M., 1995. Induction of apoptosis in catecholaminergic PC12 cells by L-DOPA. Implications for the treatment of Parkinson's disease. J. Clin. Invest. 95, 2458–2464.

Whitehead, R.E., Ferrer, J.V., Javitch, J.A., Justice, J.B., 2001. Reaction of oxidized dopamine with endogenous cysteine residues in the human dopamine transporter. J. Neurochem. 76, 1242–1251.

Xu, Y., Stokes, A.H., Roskoski Jr., R., Vrana, K.E., 1998. Dopamine, in the presence of tyrosinase, covalently modifies and inactivates tyrosine hydroxylase. J. Neurosci. Res. 54, 691–697.

Zecca, L., Zucca, F.A., Wilms, H., Sulzer, D., 2003. Neuromelanin of the substantia nigra: a neuronal black hole with protective and toxic characteristics. Trends Neurosci. 26, 578–580.

CME

Zonisamide improves motor function in Parkinson disease

A randomized, double-blind study

Miho Murata, MD, PhD; Kazuko Hasegawa, MD, PhD; Ichiro Kanazawa, MD, PhD; and The Japan Zonisamide on PD Study Group*

Abstract—*Objective:* To evaluate the efficacy, safety and tolerability of daily doses of 25, 50, and 100 mg of zonisamide (ZNS) administered as adjunctive treatment in patients with Parkinson disease (PD). *Methods:* We conducted a multicenter, randomized, double-blind, parallel-treatment, placebo-controlled study in Japan. Patients with PD who showed insufficient response to levodopa treatment were given placebo for 2 weeks and then treated for 12 weeks with 25, 50, or 100 mg/day of ZNS or placebo, in addition to levodopa, followed by a 2-week dose-reduction period. The primary endpoint was change from baseline in the total score of the Unified Parkinson's Disease Rating Scale (UPDRS) Part III at the final assessment point. Secondary endpoints included changes from baseline in total daily "off" time; total scores of UPDRS Parts I, II, and IV; and Modified Hoehn and Yahr Scale score. Safety analysis was based on the incidence of adverse events. *Results:* There was significant improvement in the primary endpoint in the 25-mg and 50-mg groups *vs* placebo. The duration of "off" time was significantly reduced in the 50-mg and 100-mg groups *vs* placebo. Dyskinesia was not increased in ZNS groups. The incidence of adverse effects was similar between the 25-mg, 50-mg, and placebo groups but higher in the 100-mg group. *Conclusions:* Zonisamide is safe, effective and well tolerated at 25 to 100 mg/day as an adjunctive treatment in patients with Parkinson disease.

NEUROLOGY 2007;68:45–50

Zonisamide (ZNS) (1,2-benzisoxazole-3-methanesulfonamide) is an antiepileptic drug with a long-half life ($T_{1/2}$ = 62 hours) that was originally synthesized in Japan.[1] ZNS has been used to treat epilepsy in Japan for more than 10 years; is currently approved for marketing in the United States, Europe, and Korea; and is generally well tolerated. We reported previously that ZNS has beneficial effects on PD in one patient with convulsion attacks.[2] Based on this finding, we subsequently performed an open trial in nine patients with PD and found that ZNS improved the main symptoms of PD, with particular benefits on motor fluctuation, known as "wearing-off."[2] Then, we conducted a small double-blind study that showed a daily dose of 50 to 100 mg of ZNS as an adjunct therapy significantly improved limb rigidity, tremor, and postural instability in patients with advanced PD and was well tolerated.[3]

In this study, we sought to confirm ZNS effectiveness as an adjunctive treatment for PD by evaluating the efficacy, safety, and tolerability of daily oral doses of 25, 50, and 100 mg of ZNS (once a day) in a large population of patients with PD who showed insufficient response to levodopa treatment.

Additional material related to this article can be found on the *Neurology* Web site. Go to www.neurology.org and scroll down the Table of Contents for the January 2 issue to find the title link for this article.

Methods. This was a multicenter, randomized, double-blind, parallel-treatment, placebo-controlled study of ZNS as adjunctive treatment in patients with PD who showed insufficient response to levodopa (including dopa decarboxylase inhibitor: DCI combination drugs). Fifty-eight institutions throughout Japan participated in the study during the study period of January 15 to December 1, 2004.

Patients with PD of both sexes between ages 20 and 80 years were enrolled in the study. Patients who exhibited any problems based on levodopa therapy, such as wearing-off phenomena, "on"–"off" phenomena, and freezing phenomena, no-"on" and delayed-"on," or in whom the suboptimal dose of levodopa had been administered because of side effects or therapeutic strategy were not excluded from the study. Patients had received individual dosages of levodopa (plus a DCI) and were stable for at least 28 days before study initiation. Patients who fulfilled the above criteria were enrolled into the study by the investigators at each participating institution. Patients who met the above criteria and provided informed consent were randomized into the treatment groups of 25, 50, or 100 mg/day ZNS or placebo.

The study consisted of a 2-week run-in period of single-blind treatment with placebo, a 12-week double-blind treatment period, and a 2-week double-blind dose-reduction period (figure E-1 on the Neurology Web site at www.neurology.org), with the exception

*See the appendix for a full list of study participants.

From the Department of Neurology (M.M., I.K.), Musashi Hospital, National Center of Neurology and Psychiatry, Tokyo, Japan; and Division of Neurology (K.H.), Sagamihara Hospital, Kanagawa, Japan.

Disclosure: Sponsored by Dainippon Sumitomo Pharma. All authors have agreed to the conditions noted on the Author Disclosure Form.

Received January 6, 2006. Accepted in final form September 25, 2006.

Address correspondence and reprint requests to Dr. Miho Murata, Department of Neurology, Musashi Hospital, National Center of Neurology and Psychiatry, 4-1-1 Ogawahigashimachi, Kodaira, Tokyo 187-8551, Japan; e-mail: mihom@ncnp.go.jp

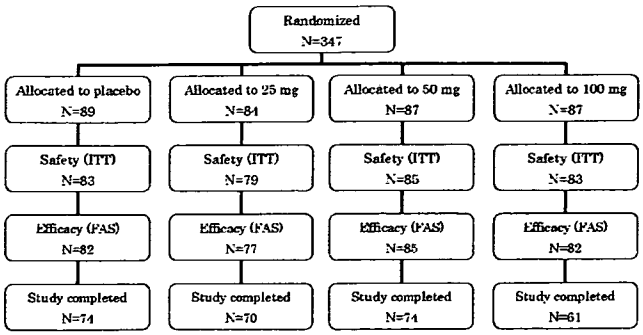

Figure 1. Patient disposition. ITT = intent-to-treat; FAS = full analysis set.

that the 25-mg group did not undergo dose reduction. Baseline assessment was conducted after a 2-week run-in period to reduce placebo effects. Clinical assessment including the Unified Parkinson's Disease Rating Scale (UPDRS) and Hoehn and Yahr staging was conducted at "on" state every 2 weeks.

The daily dosage was administered orally once a day in the morning as four tablets in the run-in and treatment periods and two tablets in the dose-reduction period. Study medication was dispensed as ZNS 25 mg tablets or matching placebo. Patients were randomized to one of the four treatment groups in blocks of size 8 (2 patients per group) during the run-in period using a randomization code generated by the study sponsor or designee. Study medication, indistinguishable by appearance, packaging, and labeling, was provided to each institution, and 1-week supplies were dispensed to patients according to the randomization code.

Patients were required to have concomitant administration with levodopa preparations including DCI combination drugs and were allowed to continue with other anti-Parkinson medications, such as dopamine receptor agonists (DAs), monoamine oxidase type B (MAO-B) inhibitors, anticholinergics, amantadine, or droxydopa, during the study. The dose regimens of these concomitant medications were to be maintained from 4 weeks before study initiation until the end of the dose-reduction period, except as required to alleviate dyskinesia or psychotic symptoms that were likely caused by dopaminergic-receptor hyperstimulation due to concomitant medication.

The primary endpoint was a change from baseline in the total score of UPDRS Part III (motor examination score) at the final assessment point. Secondary endpoints included a change from baseline in total daily "off" time as determined from patients' diaries, and changes from baseline in UPDRS Part I, II, and IV scores and Modified Hoehn and Yahr Scale score. Changes from baseline at the assessment point were analyzed by analysis of covariance using treatment group as a factor, and baseline value and treatment group scores were compared with placebo using the Dunnett test. A significance level of 0.05 (two-sided) was used for intergroup comparison, except for homogeneity assessment, when a significance level of 0.15 (two-sided) was used. The planned sample size of 80 patients per group (320 patients in total) was selected based on a requirement of 69 patients per group to achieve 80% power for comparison between placebo and each of the ZNS groups, assuming a between-group difference of 5.5 and an SD of 10.0 on the primary endpoint as seen in a preliminary study.[3] Multiplicity was taken into consideration in the primary analysis, but not in the secondary analysis or assessment of the dose–response relationship. Subgroup subset analysis was performed for the primary endpoint. Safety assessment was based on the incidence of adverse events including abnormalities of clinical/laboratory examinations and the incidence compared between the treatment groups by χ^2 test. Demographic and efficacy analyses were performed on the full analysis set (FAS), and safety assessments were performed on the intent-to-treat (ITT) population.

Results. Patient disposition is summarized in figure 1. Of the 347 screened and randomized patients, 279 patients (80.4%) completed the protocol as planned. There were no major differences between groups except that markedly fewer patients in the ZNS 100 mg group completed the study. The ITT population consisted of 330 patients (95.1%), with 83 patients in the placebo group, 79 in the 25-mg group, 85 in the 50-mg group, and 83 in the 100-mg group. A total of 6 patients in the placebo group, 5 in the 25-mg group, 2 in the 50-mg group, and 4 in the 100-mg group were not included in the ITT population because of withdrawal of consent or dosing regimen violation. The FAS consisted of the ITT minus 4 patients: 2 in the 25-mg group and 1 in each of the placebo and 100-mg groups because of no efficacy data during and after treatment period. Of the 326 patients (FAS), 279 patients completed the therapy period, and 47 patients discontinued therapy prematurely (8 patients in the placebo group, 7 in the 25-mg group, 11 in the 50-mg group, and 21 in the 100-mg group). The most common reason for discontinuation was adverse events (4 patients in the placebo group, 5 in the 25-mg group, 4 in the 50-mg group, and 9 in the 100-mg group). There were no Good Clinical Practice deviations in this study.

Table 1 shows the demographic background of patients in the placebo and ZNS treatment groups. There were no major differences between groups with respect to patients' background, including disease and treatment histories. The mean morbidity period was 8.6 years, and the mean modified Hoehn and Yahr Scale score ("on") was 2.5. The mean number of concomitant anti-Parkinson medicines was 3.2. The most common concomitant medications were DAs, which were used by 91.7% of the patients, and MAO-B inhibitors, which were used by 51.5% of the patients.

The changes (least-squares mean ± SE) in UPDRS Part III total score from baseline at final assessment were as follows: placebo group, −2.0 ± 0.8; 25-mg group, −6.3 ± 0.8; 50-mg group, −5.8 ± 0.8; and 100-mg group, −4.6 ± 0.8 (figure 2). All treatment groups showed decreases of UPDRS Part III total scores from baseline, but the improvement was significant for the 25-mg ($p = 0.001$, Dunnett test) and 50-mg ($p = 0.003$, Dunnett test) groups, vs the placebo group.

The proportions of responders, defined as patients with ≥30% reduction in UPDRS Part III total score from baseline at final assessment, were as follows: placebo group, 22.0% (18/82); 25-mg group, 35.1% (27/77, $p = 0.067$, χ^2 test vs placebo group); 50-mg group, 38.8% (33/85, $p = 0.018$, χ^2 test vs placebo group); and 100-mg group, 31.7% (26/82, $p = 0.158$, χ^2 test vs placebo group).

The degree of change for the primary endpoint were similar in the 25-mg and 50-mg groups, and these were greater than in the 100-mg group and significantly greater than in the placebo group. Subgroup analyses indicated no significant effects in subject baseline characteristics including with or without MAO-B inhibitor (table E-1) on the primary endpoint.

The mean decrease in total "off" time from baseline at final assessment is shown in figure 3. The mean changes in "off" time (hours) from baseline were as follows: placebo group, −0.20 (n = 61); 25-mg group, −0.22 (n = 58); 50-mg group, −1.30 (n = 68); and 100-mg group, −1.63 (n = 52). The duration of daily "off" time decreased for all treatment groups with improvement in the 50-mg ($p = 0.014$, Dunnett test) and 100-mg ($p = 0.013$, Dunnett test) groups compared with the placebo group.

Table 1 Demographic and baseline characteristics of patients according to the dose of zonisamide

		ZNS		
	Placebo	25 mg/day	50 mg/day	100 mg/day
n	82	77	85	82
Age, years	65.3 (7.5)	65.1 (8.5)	63.9 (9.4)	65.7 (8.6)
Older than 65 years	47 (57.3%)	42 (54.5%)	46 (54.1%)	53 (64.6%)
Men	41 (50.0%)	42 (54.5%)	51 (60.0%)	47 (57.3%)
Duration of PD, years	8.9 (5.8)	8.5 (4.6)	8.6 (6.0)	8.5 (5.6)
Dose of l-dopa, mg/day	351.2 (138.8)	355.5 (115.6)	363.9 (177.4)	327.7 (118.2)
Wearing-off	67 (81.7%)	64 (83.1%)	74 (87.1%)	62 (75.6%)
Dyskinesia	28 (34.1%)	18 (23.4%)	33 (38.8%)	22 (26.8%)
+ Dopamine agonist	80 (97.6%)	76 (98.7%)	85 (100.0%)	80 (97.6%)
+ MAO-B inhibitor	42 (51.2%)	38 (49.4%)	43 (50.6%)	45 (54.9%)
UPDRS Part III	22.9 (10.7)	26.5 (13.0)	22.5 (13.1)	22.7 (11.6)
H-Y ("on")	2.60 (0.72)	2.68 (0.76)	2.49 (0.80)	2.60 (0.77)
H-Y ("off")	3.52 (0.80)	3.64 (0.80)	3.49 (0.90)	3.40 (0.77)
"Off" time, hours	7.13 (3.45)	6.76 (3.13)	6.51 (2.30)	7.62 (3.03)

Data are mean (SD) or number (%).

ZNS = zonisamide; PD = Parkinson disease; H-Y = Modified Hoehn and Yahr Scale score.

There were no significant differences between the ZNS and placebo groups with respect to changes from baseline in UPDRS Parts I, II, and IV scores and in the Modified Hoehn and Yahr Scale score.

Some patients showed increased duration of dyskinesia with increase of "on" time; however, the frequency of dyskinesia was not increased in the entire ZNS group compared with the placebo group. Further analysis showed a decrease in disabling dyskinesia (UPDRS Part IV, No. 33) in the 50-mg group (table 2). In addition, the basal dose of levodopa did not correlate with worsening or improvement of dyskinesia.

There was no significant difference in incidence of adverse events between the 25-mg (a total of 164 adverse events reported by 70.9% [56/79] of the patients) and 50-mg (195 adverse events reported by 72.9% [62/85] of the patients) groups, compared with the placebo group (153 adverse events by 65.1% [54/83] of the patients). However, the incidence of adverse events was significantly higher in the 100-mg group (204 adverse events reported by 79.5% [66/83] of the patients) compared with the placebo group ($p = 0.037$, χ^2 test). Adverse events with an incidence of greater than 5% in the ZNS group are presented in table 3. Adverse events for which the incidence was greater in the total ZNS than in the placebo group were somnolence (10.9%), apathy (8.5%), decrease in body weight (6.9%), and constipation (6.5%). Adverse events for which the incidence in the total ZNS was less than that of the placebo

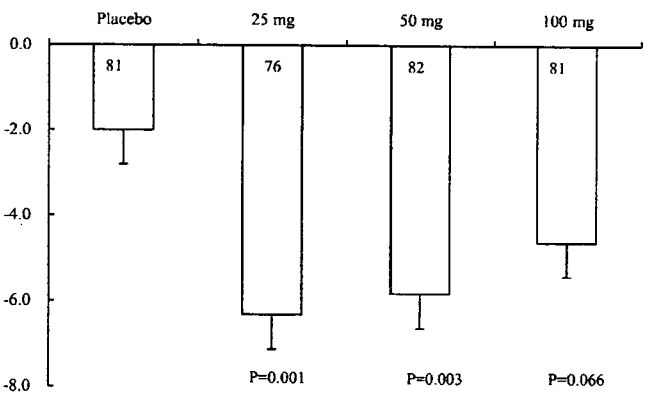

Figure 2. Changes in Unified Parkinson's Disease Rating Scale (UPDRS) Part III total score induced by zonisamide (ZNS) treatment from baseline to end of study (least-squares mean ± SE). Numbers indicate patient numbers. The total score of UPDRS Part III decreased after treatment in the 25-mg/day ($p = 0.001$) and 50-mg/day ($p = 0.003$) ZNS groups compared with the placebo group.

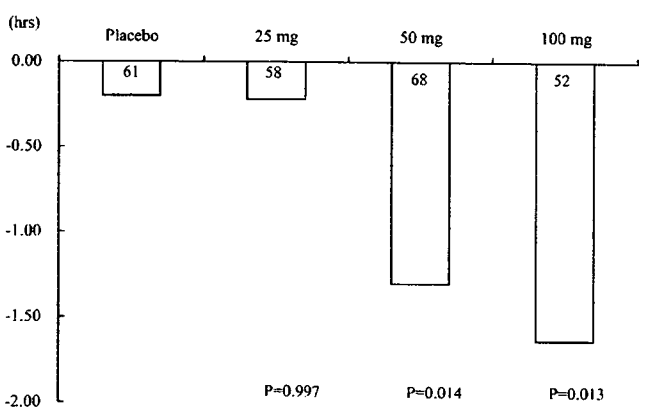

Figure 3. Changes from baseline in mean daily "off" time (hours) induced by treatment with zonisamide (ZNS). Numbers indicate patient numbers. "Off" time decreased after treatment with ZNS in the 50-mg/day (−1.3 hours, $p = 0.014$) and 100-mg/day (−1.63 hours, $p = 0.013$) groups compared with the placebo group.